

**Optical Variability Correlated with X-ray Spectral Transition
in the Black-Hole Transient ASASSN-18ey = MAXI J1820+070**

Keito Nijjima¹, Mariko Kimura¹, Yasuyuki Wakamatsu¹, Taichi Kato¹, Daisaku Nogami¹, Keisuke Isogai¹, Naoto Kojiguchi¹, Ryuhei Ohnishi¹, Megumi Shidatsu², Geoffrey Stone³, Franz-Josef Hamsch^{4,5,6}, Tamás Tordai⁷, Michael Richmond⁸, Tonny Vanmunster^{9,10}, Gordon Myers¹¹, Stephen M. Brincat¹², Pavol A. Dubovsky¹³, Tomas Medulka¹³, Igor Kudzej¹³, Stefan Parimucha¹⁴, Colin Littlefield¹⁵, Berto Monard^{16,17}, Joseph Ulowetz¹⁸, Elena P. Pavlenko¹⁹, Oksana I. Antonyuk¹⁹, Aleksei A. Sosnovskij¹⁹, Aleksei V. Baklanov¹⁹, Kirill A. Antoniu¹⁹, Nikolai V. Pit¹⁹, Sergei P. Belan¹⁹, Julia V. Babina¹⁹, Aleksandr S. Sklyanov²⁰, Anna M. Zaoztrozhnykh²¹, Andrew V. Simon²², Lewis M. Cook²³, Ian Miller²⁴, Hiroshi Itoh²⁵, Domenico Licchelli^{26,27}, Shawn Dvorak²⁸, Richard Sabo²⁹, Yenel Ögmen³⁰, Donn R. Starkey³¹, Peter Nelson³², Enrique de Miguel^{33,34}, Charles Galdies³⁵, Kenneth Menzies³⁶, Seiichiro Kiyota³⁷, Arto Oksanen³⁸, Roger D. Pickard^{39,40}, Alexandra M. Zubareva^{41,42}, Klaus Wenzel⁵ & Denis Denisenko⁴²

¹ Department of Astronomy, Graduate School of Science, Kyoto University,
Oiwakecho, Kitashirakawa, Sakyo-ku, Kyoto 606-8502, Japan

² Department of Physics, Ehime University, 2-5, Bunkyocho, Matsuyama, Ehime 790-8577, Japan

³ American Association of Variable Star Observers, 49 Bay State Rd., Cambridge, MA 02138, USA

⁴ Groupe Européen d'Observations Stellaires (GEOS), 23 Parc de Levesville, 28300 Bailleau l'Évêque, France

⁵ Bundesdeutsche Arbeitsgemeinschaft für Veränderliche Sterne (BAV), Munsterdamm 90, 12169 Berlin, Germany

⁶ Vereniging Voor Sterrenkunde (VVS), Oude Bleken 12, 2400 Mol, Belgium

⁷ Polaris Observatory, Hungarian Astronomical Association, Laborc utca 2/c, 1037 Budapest, Hungary

⁸ Physics Department, Rochester Institute of Technology, Rochester, New York 14623, USA

⁹ Center for Backyard Astrophysics Belgium, Walhostraat 1A, B-3401 Landen, Belgium

¹⁰ Center for Backyard Astrophysics Extremadura, 06340 Fregenal de la Sierra, Spain

¹¹ Center for Backyard Astrophysics San Mateo, 5 Inverness Way, Hillsborough, CA 94010, USA

¹² Flarestar Observatory, Fl.5/B, George Tayar Street, San Gwann SGN 3160, Malta

¹³ Vihorlat Observatory, Mierova 4, 06601 Humenne, Slovakia

¹⁴ Institute of Physics, Faculty of Science, UPJS Kosice, Slovakia

¹⁵ Department of Physics, University of Notre Dame,

225 Nieuwland Science Hall, Notre Dame, Indiana 46556, USA

¹⁶ Bronberg Observatory, Center for Backyard Astrophysics Pretoria,

PO Box 11426, Tiegterpoort 0056, South Africa

¹⁷ Kleinkaroo Observatory, Center for Backyard Astrophysics Kleinkaroo,

Sint Helena 1B, PO Box 281, Calitzdorp 6660, South Africa

¹⁸ Center for Backyard Astrophysics Illinois, Northbrook Meadow Observatory,

855 Fair Ln, Northbrook, Illinois 60062, USA

¹⁹ Federal State Budget Scientific Institution Crimean Astrophysical Observatory of RAS,

Nauchny, 298409, Republic of Crimea

- ²⁰ Kazan (Volga region) Federal University, Kremlevskaya str., 18, Kazan, 420008, Russia
- ²¹ Institute of Physics, Kazan Federal University, Ulitsa Kremlevskaya 16a, Kazan 420008, Russia
- ²² Astronomy and Space Physics Department, Taras Shevshenko National University of Kyiv,
Volodymyrska str. 60, Kyiv, 01601, Ukraine
- ²³ Center for Backyard Astrophysics Concord, 1730 Helix Ct. Concord, California 94518, USA
- ²⁴ Furzehill House, Ilston, Swansea, SA2 7LE, UK
- ²⁵ Variable Star Observers League in Japan (VSOLJ), 1001-105 Nishiterakata, Hachioji, Tokyo 192-0153, Japan
- ²⁶ R.P. Feynman Observatory, Gagliano del Capo, 73034, Italy
- ²⁷ CBA, Center for Backyard Astrophysics - Gagliano del Capo, 73034, Italy
- ²⁸ Rolling Hills Observatory, 1643 Nightfall Drive, Clermont, Florida 34711, USA
- ²⁹ 2336 Trailcrest Dr., Bozeman, Montana 59718, USA
- ³⁰ Green Island Observatory, Geçitkale, Magosa, via Mersin, North Cyprus
- ³¹ DeKalb Observatory, H63, 2507 County Road 60, Auburn, IN 46706, USA
- ³² 1105 Hazeldean Rd, Ellinbank 3820, Australia
- ³³ Departamento de Ciencias Integradas, Facultad de Ciencias Experimentales,
Universidad de Huelva, 21071 Huelva, Spain
- ³⁴ Center for Backyard Astrophysics, Observatorio del CIECEM, Parque Dunar,
Matalascañas, 21760 Almonte, Huelva, Spain
- ³⁵ Institute of Earth Systems, University of Malta
- ³⁶ Center for Backyard Astrophysics (Framingham), 318A Potter Road, Framingham, MA 01701, USA
- ³⁷ VSOLJ, 7-1 Kitahatsutomi, Kamagaya, Chiba 273-0126, Japan
- ³⁸ Hankasalmi observatory, Jyvaskylan Sirius ry, Verkkoniementie 30, FI-40950 Muurame, Finlandy
- ³⁹ The British Astronomical Association, Variable Star Section (BAA VSS),
Burlington House, Piccadilly, London, W1J 0DU, UK
- ⁴⁰ 3 The Birches, Shobdon, Leominster, Herefordshire, HR6 9NG, UK
- ⁴¹ Institute of Astronomy, Russian Academy of Sciences, Moscow 119017, Russia
- ⁴² Sternberg Astronomical Institute, Lomonosov Moscow State University,
Universitetsky Ave., 13, Moscow 119992, Russia

Abstract

How a black hole accretes matter and how this process is regulated are fundamental but unsolved questions in astrophysics. In transient black-hole binaries, a lot of mass stored in an accretion disk is suddenly drained to the central black hole because of thermal-viscous instability. This phenomenon is called an outburst and is observable at various wavelengths (Frank et al., 2002). During the outburst, the accretion structure in the vicinity of a black hole shows dramatical transitions from a geometrically-thick hot accretion flow to a geometrically-thin disk, and the transition is observed at X-ray wavelengths (Remillard, McClintock, 2006; Done et al., 2007). However, how that X-ray transition occurs remains a major unsolved problem (Dunn et al., 2008). Here we report extensive optical photometry during the 2018 outburst of ASASSN-18ey (MAXI J1820+070), a black-hole binary at a distance of 3.06 kpc (Tucker et al., 2018; Torres et al., 2019) containing a black hole and a donor star of less than one solar mass. We found optical large-amplitude periodic variations similar to superhumps which are well observed in a subclass of white-dwarf binaries (Kato et al., 2009). In addition,

the start of the stage transition of the optical variations was observed 5 days earlier than the X-ray transition. This is naturally explained on the basis of our knowledge regarding white dwarf binaries as follows: propagation of the eccentricity inward in the disk makes an increase of the accretion rate in the outer disk, resulting in huge mass accretion to the black hole. Moreover, we provide the dynamical estimate of the binary mass ratio by using the optical periodic variations for the first time in transient black-hole binaries. This paper opens a new window to measure black-hole masses accurately by systematic optical time-series observations which can be performed even by amateur observers.

On March 6th, 2018, ASASSN-18ey was discovered by the All-Sky Automated Survey for SuperNovae (ASAS-SN) with an increase of optical luminosity. This object was faint about 4 days before the discovery, and hence, this sudden optical eruption was the onset of an outburst. After the detection, on March 12th, 2018, the Monitor of All-sky X-ray Image (*MAXI*) found an X-ray transient MAXI J1820+070 (Kawamuro et al., 2018) which was identified with ASASSN-18ey via optical follow-up observations (Denisenko, 2018). This object was suggested to be a black-hole binary from the X-ray spectra and the typical relation between optical and X-ray luminosity (Baglio et al., 2018). Also, very recent spectroscopic observations confirmed that the central object in this binary is a black hole by estimating the binary mass function (Torres et al., 2019).

We performed multi-color optical photometry of ASASSN-18ey = MAXI J1820+070 via the Variable Star Network (VSNET) since BJD 2,458,189 (corresponds to 2018 March 11) (Extended Data Table 1 and Methods section ‘Detailed methods of optical observations and analyses’). We also used the optical data taken by the American Association of Variable Star Observers (AAVSO). Our data are one of the densest optical data of outbursts in transient black-hole binaries in the sense that they contain >400,000 data points and cover the entire outburst that lasted for more than 200 days. We also compare our optical data with the 2.0–4.0-keV and 4.0–10.0-keV X-ray light curves taken by *MAXI*.

The overall optical and X-ray light curves of this outburst are shown in Figure 1a. The rapid rise and the exponential decay of the optical behavior seems to be typical during outburst in black-hole binaries (Tanaka, Shibazaki, 1996). We did not detect any optical periodic variations during the first 70 days. However, large-amplitude periodic oscillations appeared around BJD 2,458,260 (corresponds to 2018 March 21) and continued for ~ 145 days (Figure 1b). Here we use the two-dimensional least absolute shrinkage and selection operator (Lasso Kato, Uemura (2012)) to derive sharp peaks in power spectra from unevenly sampled data by suppressing aliases. Although the light curves of soft-X-ray outbursts in typical black-hole binaries show sudden increases at the initial stage and long plateaus lasting a few hundred days (Remillard, McClintock, 2006; Done et al., 2007), the initial increase of soft-X-ray flux was moderate in this object, and the dramatic X-ray spectral transition began ~ 100 days after the onset of the X-ray outburst.

We investigated the period and amplitude variations of the detected optical periodic variability in ASASSN-18ey (Figure 2). Their periods were always longer than the detected orbital period 0.68549(1) days, which was estimated from the radial velocities of the binary motion (Torres et al., 2019). The $O - C$ plane shown in Figure 2a represents the accumulated time difference of periods with respect to the reference period at each cycle E and is sensitive to slight period variations (Extended Data Table 2 and Methods section ‘SU UMa/WZ Sge-type stars and time evolution of their superhumps’). We found that the period was constant and that the amplitude increased during around BJD 2,458,260–2,458,290. After that, the period suddenly dropped, and gradually increased, while the amplitude gradually decreased. The positive excesses of the periods with respect to the orbital period and other characteristic features are identical to “superhumps” observed during outburst in SU UMa-type stars, a subclass of dwarf novae with small mass ratios of the donor to the primary (Kato et al., 2009). Dwarf novae are close binary systems consisting of a central white dwarf and a donor star (Warner, 1995). Superhumps have periods slightly longer than the corresponding orbital period, and the periods vary with time. They are believed to be generated by a periodic tidal dissipation in the precessing eccentric disk which is produced by tidal instability working in binaries having mass ratios smaller than 0.25 (Methods section ‘SU UMa/WZ Sge-type stars and time evolution of their superhumps’). Hereafter, we call the constant-period stage “stage A” and the varying-period stage “stage B”, following the notation in the field of dwarf novae (Methods section ‘SU UMa/WZ Sge-type stars and time evolution of their superhumps’).

As stated above, dwarf novae have accretion disks just like black-hole binaries. Since these objects have the different scale and temperature but have the similar structure, dwarf novae are sometimes called “a miniature version of black-hole binaries” (Kuulkers et al., 1996). Taking this similarity into consideration, it is expected that the physics of an accretion disk of a black-hole binary may be understood by analogy to the underlying physics of superhumps in dwarf novae.

Although superhump candidates have been reported only in several black-hole binaries prior to this work,

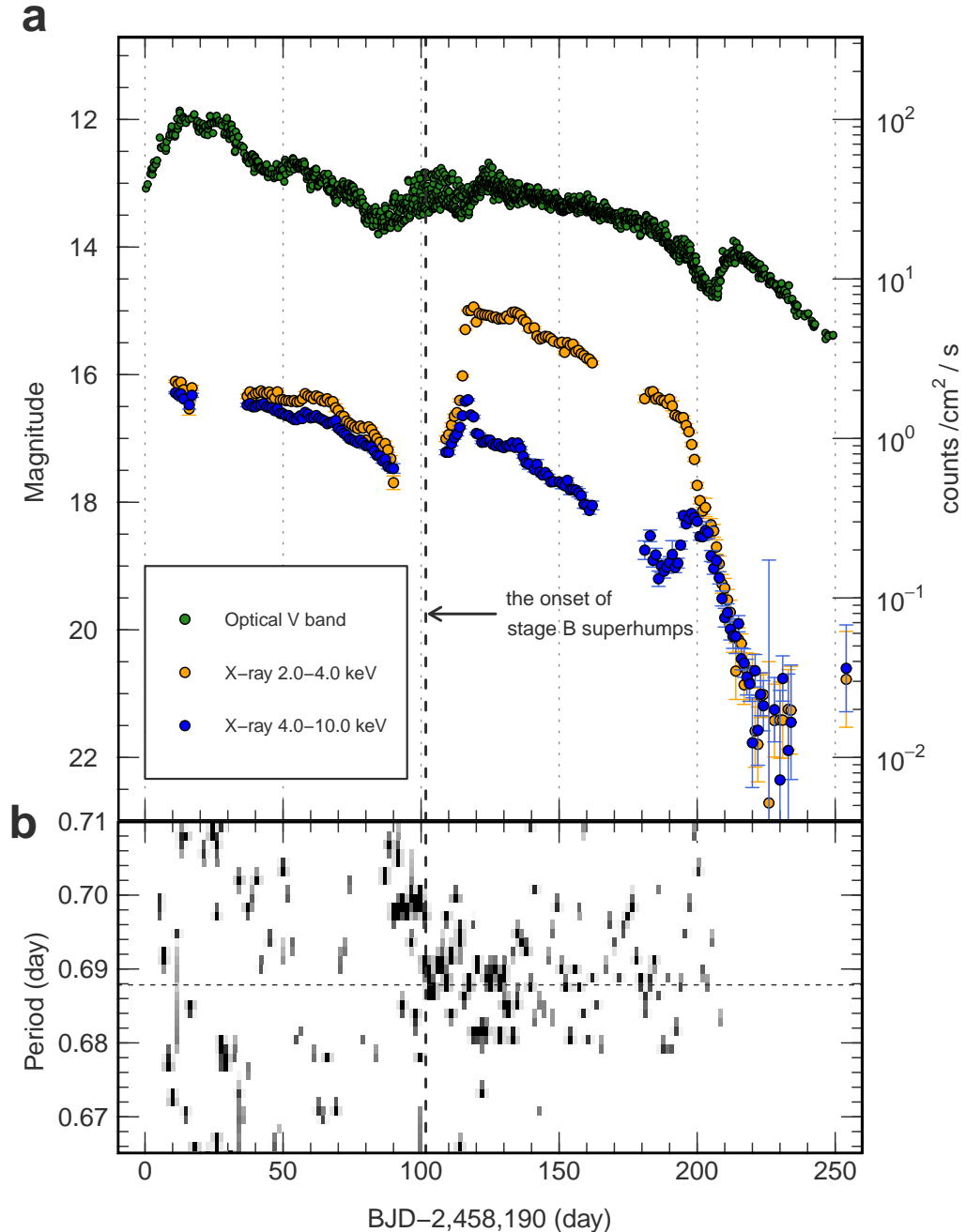


Figure 1: **Overall light curves of ASASSN-18ey and the two-dimensional power spectral density by Lasso.** Panel (a) shows optical V-band and MAXI X-ray light curves of ASASSN-18ey during Barycentric Julian Day (BJD) 2,458,189–2,458,440. The horizontal and vertical axis represents BJD-2,458,190 and Magnitude respectively. The vertical dashed line represents the onset of stage B superhumps. There seems to be a relation between the X-ray state transition and the change of superhump stage. Error bars in the X-ray light curves represent 1σ confidence intervals. The errors in optical light curve are equal or smaller than the size of the points. Panel (b) shows the time-varying periods calculated by Lasso which can derive a sharp peak from a sparse light curve. The vertical axis represents the period. Once the superhumps started, the characteristic period appeared.

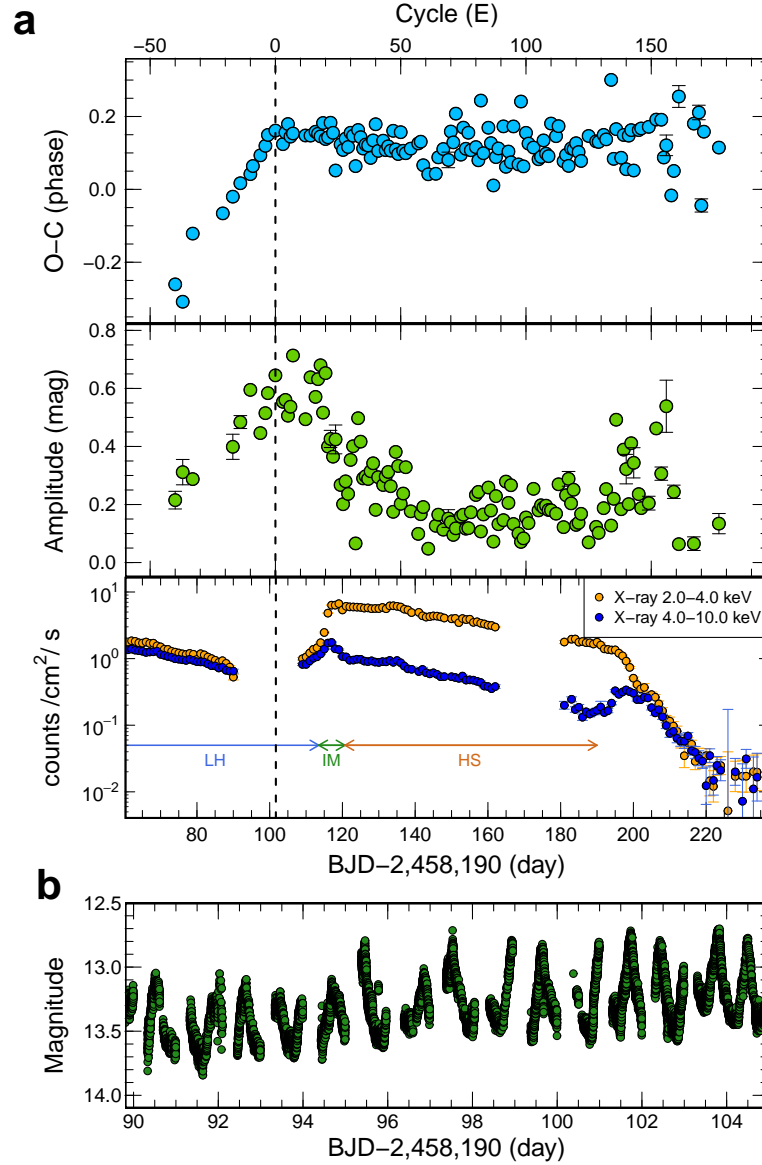


Figure 2: **The comparison of the stage of superhumps and X-ray state transition in ASASSN-18ey.** (a) Upper: The $O - C$ of ASASSN-18ey, which expresses the time variation of the period of superhumps. Middle: The variation of the amplitude of superhumps. Bottom: The X-ray light curves of ASASSN-18ey. In these panels, the error bars represent 1σ confidence intervals. On BJD 2,458,291.7 denoted by the vertical dashed line, there is a clear bending point on the $O - C$ and the amplitude planes, which means that the X-ray hard-to-soft state transition is a slightly delayed with respect to the stage transition of superhumps. The X-ray spectral state reported by Shidatsu et al. (2019) is also denoted in the bottom panel and “LH”, “IM”, and “HS” stand for the low-hard state, the intermediate (very high state), and the high-soft state, respectively. We here use $C = 2458261.952323 + 0.688907 E$. (b) The light curve of superhumps during stage A. The single-peaked humps are clearly observed. The amplitude is ~ 0.8 mag and the averaged period is ~ 0.697 days.

nobody found clearly their period variations (Methods section ‘Black-hole binaries showing superhump candidates in the past’). Our study establishes the presence of superhumps as a process that may affect black-hole X-ray binaries that undergo canonical evolution through multiple accretion states during an outburst. Although the averaged amplitudes and period of superhumps in SU UMa stars are typically ~ 0.25 mag and less than 0.1 days, respectively (Kato et al., 2012), those of ASASSN-18ey are much larger (~ 0.8 mag) and longer (~ 0.69 days). The long period of superhumps is naturally expected from the orbital period of this system (Torres et al., 2019), which is much longer than typical orbital periods in SU UMa-type dwarf novae. On the other hand, we predict the superhump amplitude should be ~ 0.07 mag in this system if the intrinsic superhump amplitude is the same as the averaged amplitude in SU UMa stars and the greater X-ray irradiation of ASASSN-18ey is accounted for. The superhumps caused by the tidal dissipation are thus detectable against previous suggestions (Haswell et al., 2001). However, the expected amplitude is smaller than the observational one. The ~ 100 -times larger disk than the averaged one in SU UMa stars and/or the change of the surface area receiving X-rays from the inner disk might contribute to the large amplitude of the superhumps (Figure 7 and Methods section ‘SED modelling’).

We estimated the period of stage A superhumps to be 0.7029(3) days by using the data during BJD 2,458,263.7–2,458,291.7 (corresponds to 2018 May 25.2–2018 June 22.2). Then we were able to estimate the binary mass ratio (q) of this object to be 0.066(1) from the stage A superhump period and the identified orbital period (Torres et al., 2019) by the dynamical method for mass-ratio estimations, which is based on a well-established treatment of celestial mechanics and is verified in the study of dwarf novae (Kato, Osaki, 2013) (Methods section ‘Estimation of black-hole masses with stage A superhumps’). The old method proposed by Patterson et al. (2005) is not suitable, since it is based on the empirical relation between the orbital period and the period of time-varying stage B superhumps. It was proved that this method easily underestimate the binary mass ratio (Nakata et al., 2013). Our estimate is more accurate than ever because we used stage A superhumps only. Since the spectral type of the donor is constrained to be K late type, the donor mass is $0.59^{+0.11}_{-0.10} M_{\odot}$ (Torres et al., 2020), where M_{\odot} is the solar mass. Therefore the black-hole mass is estimated to be $7.3\text{--}10.8 M_{\odot}$. This is consistent with the black-hole mass estimated from the rotational velocity to be $8.48^{+0.79}_{-0.72} M_{\odot}$ (Torres et al., 2020).

Also, we obtain 0.047–0.093 as the value of the mass ratio, which infers the black-hole mass to be $5.3\text{--}12.2 M_{\odot}$, by using a relation between the duration of stage A superhumps and the mass ratio (Figure 3; Methods section ‘Estimation of black-hole masses with stage A superhumps’). This relation is based on the theory (Lubow, 1991) that the growth time of superhumps is proportional to q^{-2} , and has also been confirmed observationally (Methods section ‘Estimation of black-hole masses with stage A superhumps’). The duration of the stage A superhumps in ASASSN-18ey is estimated to have been 71 cycles if the epoch at which the superhump amplitude should have been zero is BJD 2,458,238.5 (corresponds to 2018 April 30.0). We have derived this epoch by the linear regression of the data before BJD 2,458,291.7 which is displayed in the second panel of Figure 2a and have calculated the cycle length by dividing the estimated stage A superhump duration by its period. We have substituted this estimate into the relation denoted by the black solid line in Figure 3, which is derived by the linear regression of the orange circles in the same figure. We consider the error of the regression to obtain the mass ratio of ASASSN-18ey. The estimated range of the black-hole mass covers that derived by the former method.

The inclination angle is estimated to be ~ 60 deg from our estimates of the binary mass ratio, if we assume the mass function of ASASSN-18ey is ~ 5.18 (Torres et al., 2019). This result is consistent with no confirmed eclipsing events in this system and the estimated orientation of the radio jet (Atri et al., 2020), although the inferred inclination by (Torres et al., 2020) is arrowed to exceed 66 deg. Torres et al. (2019) assumed that ASASSN-18ey shows the grazing eclipse, and constrained the inclination; however, there are no signs of that eclipse in our extensive photometry. The inclination angle should be smaller than their estimate as we have derived above. Also, they used the old method for estimating the binary mass ratio. This is the reason why our estimate of the black-hole mass is deviated from their result. The recent remarkable development of time-domain astronomy will provide plenty of optical light curves during bright outbursts, and hence, the black-hole-mass estimations in transient sources by the two methods using stage A superhumps will be rapidly spread.

Interestingly, the stage A to B transition of superhumps occurred nearly at the same time as the beginning of the hard-to-soft state transition of X-ray spectra (Figure 2a). From these panels that the rapid increase of soft X-ray flux around BJD 2,458,300 (corresponds to 2018 June 30) seems to have been almost coincident with the onset of stage B superhumps but delayed for ~ 10 days. The estimated disk radius during stage B superhumps by broadband SED analyses is $\sim 10^5 r_{\text{g}}$ (Methods section ‘SED modelling’), and the delay timescale is consistent with the viscous timescale at that radius (Meyer, 1984). Here, r_{g} indicates the gravitational radius defined as GM_1/c^2 . Before the X-ray state transition, an optically-thick hot accretion flow (Narayan, Yi, 1994; Esin et al.,

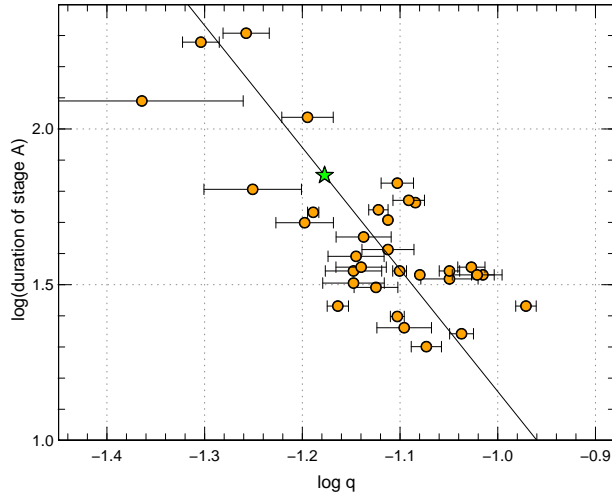


Figure 3: **The estimations of the binary mass ratio by stage A superhumps.** The relation between the duration of stage A and the mass ratio q . The vertical axis is the duration of stage A (cycle) in log scale and the horizontal axis is mass ratio in log scale. The orange points represent WZ Sge-type objects. The oblique line is the result of a linear regression analysis. Using this relation, ASASSN-18ey is located at the green point from its duration of stage A. Its mass ratio, therefore, can be obtained and the value is 0.065–0.071. This error comes from the indeterminateness of the duration of stage A (we postulated that the duration is 50–60 cycles). The error bars represent 1σ confidence intervals.

1997) producing hard photons was located above the inner disk and/or inside a truncated disk and governed the X-ray spectra (Shidatsu et al., 2018; Kara et al., 2019; Shidatsu et al., 2019). However, our SED analyses and other works suggest the inner disk outshone the hot corona after the transition during stage B superhumps (Figure 7 and Methods section ‘SED modelling’). We interpret that the mass accretion rate suddenly rose by a factor of $\gtrsim 2$ after the state transition under the assumption of almost constant radiative efficiency (Shidatsu et al., 2019). The X-ray delay at the onset of this outburst also had a similar timescale, and is regarded as the viscous timescale of the large disk.

We suggest that the tidal instability would contribute to the sudden appearance of a luminous innermost disk at the dramatic hard-to-soft X-ray state transition. The observed superhumps, our mass-ratio estimation, and the optical behavior of the overall outburst strongly suggest that the tidal instability worked during the 2018 outburst of ASASSN-18ey in addition to the thermal-viscous instability (Methods section ‘Overall optical behavior’). The tidal instability is believed to cause not only the disk precession but also the increase in mass accretion rates (Osaki, 1989). We show in Figure 4 the schematic picture of the time evolution of the accretion disk when the tidal instability works. Once the tidal instability is triggered, the non-axisymmetric perturbation is amplified. Eccentricity gradually develops only at the outermost ring of a disk, and the periodic tidal dissipation by the donor in the prograde precessing disk causes stage A superhumps. Once the precessing ring is formed, the removal of the angular momentum becomes highly efficient at the outermost ring and the mass accretion is locally enhanced. The increase in the mass accretion rate then propagates inwards and causes a global increase in mass accretion rates after a viscous time simultaneously with the development of stage B superhumps regarded as the onset of the inward propagation of the eccentricity (Kato, Osaki, 2013). We interpret that this process occurred in the 2018 outburst of ASASSN-18ey; the accretion rate at the outer disk was firstly raised by the efficient angular-momentum removal and it propagated to the innermost region of the disk over ~ 10 days, which induced the dramatic increase of soft-X-ray flux.

The following works support our interpretation. The numerical simulation of the outbursts of X-ray transient systems show the mass accretion rate onto the central star rapidly rises after the onset of the tidal instability (Ichikawa et al., 1994). Also, the same kind of interpretation that the effect of tidal instability penetrates towards the innermost disk is proposed in dwarf-nova studies from the softening of X-ray spectra confirmed in a

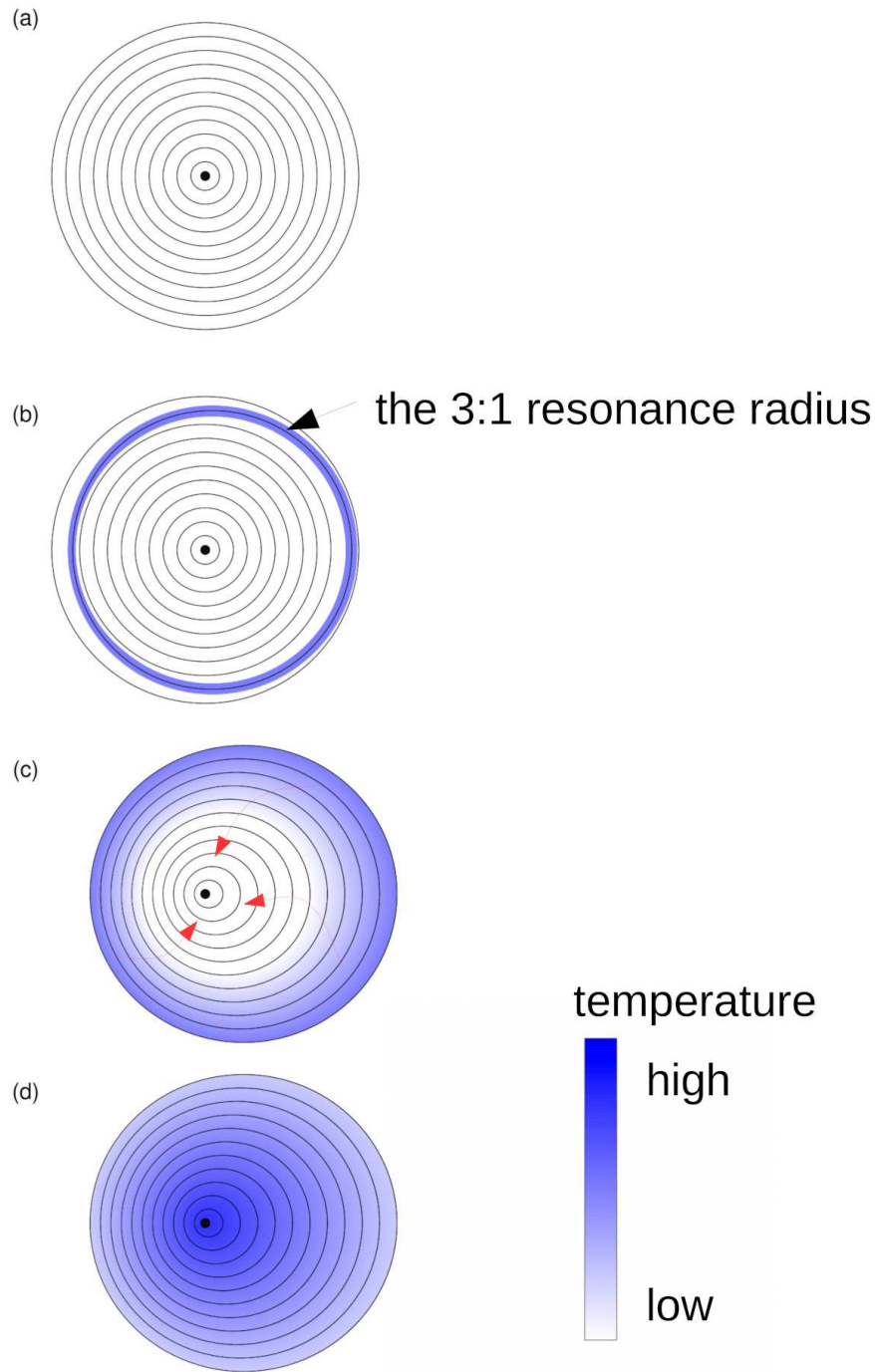


Figure 4: **The evolution of accretion correlated with the time-varying superhump behavior.** The schematic picture of the time evolution of accretion in a disk, which is expected to be similar to that in dwarf novae. In each picture from (a) to (d), the central black points represent white dwarfs. The darker the color is, the higher the temperature is. (a) The temperature is low at the outer rim, and smoothly increases inwards in a steady-state disk. (b) The disk matter at the 3:1 resonance radius, which rotates around the white dwarf three times while the donor revolves once, is affected by a tidal force from the donor. When the stage A superhumps develop, the ring around the 3:1 resonance radius suffers from the enhanced tidal torque, and becomes eccentric. Every time the donor arrives at the periastron of the elliptical disk, the angular momentum loss at the outer disk is enhanced and the accretion rate becomes higher locally. (c) At the end of stage A superhumps, the local variations of mass accretion rates propagate inwards as well as the inward propagation of eccentricity. Then, the superhump behavior moves towards the state called stage B. (d) Finally, the disk becomes steady, and the temperature of the whole disk is higher than the temperature in state (a).

well-observed WZ Sge-type DN just after the stage A to B transition of superhumps (Neustroev et al., 2018). The delay of superhump appearance is considered to depend on the binary mass ratio and the accumulated mass in the disk before each outburst (Osaki, Meyer, 2002). Our proposed interpretation could also explain the variety in the timing of the X-ray spectral transition including the standard hard-to-soft transition. This study therefore proposes one of the possible scenarios of a long standing question in high-energy astrophysics, “what the trigger of the dramatic X-ray spectral transition is” in transient low-mass X-ray binaries (Dunn et al., 2008; Shidatsu et al., 2019).

Acknowledgements

We acknowledge the variable star observations from the AAVSO International Database contributed by observers worldwide and used in this research. This work was financially supported by Grants-in-Aid for JSPS Fellows for young researchers (M. Kimura and K. Isogai).

Author Contributions

K.N. and Y.W. led the campaign. K.N. performed optical data analysis and compiled all optical data. M.K., N.K., and K.I. performed optical data analysis. M.K., T.K., D.N., and M.S. contributed to science discussions. M.K. performed multi-wavelength data analysis. Other authors than those mentioned above performed optical observations. K.N., M.K., and Y.W. wrote the manuscript. T.K. supervised this project. K.N., M.K., T.K., W.Y., M.S., J.U., C.G., D.D., M.R., R.P., F.H., E.M. and C.L. improved the manuscript. All authors have read and approved the manuscript.

Competing Interests

The authors declare that they have no competing financial interests.

Author Information

Correspondence and requests for materials should be addressed to K.N. (nijjima@kusastro.kyoto-u.ac.jp).

METHODS

1 Detailed methods of optical observations and analyses

After the onset of the 2018 outburst of ASASSN-18ey, the VSNET collaboration team (Kato et al., 2004) started a worldwide photometric campaign. Time-resolved CCD photometry was carried out at 32 sites using 32 telescopes with apertures of dozens of centimeters. We also used the public AAVSO data¹. We corrected for bias and flat-fielding in the usual manner, performed standard aperture photometry, and measured magnitudes of ASASSN-18ey relative to local comparison stars whose magnitudes were measured by A. Henden (sequence 15167RN) from the AAVSO Variable Star Database (Henden et al., 2016)². We applied small zero-point corrections to some observers’ measurements. The typical exposure time was 50 seconds. All of the observation times were converted to Barycentric Julian Date (BJD).

We performed the period analyses with the phase dispersion minimization method (PDM) (Stellingwerf, 1978). In the analyses, the global trend of the light curves is subtracted by locally weighted polynomial regression (LOWESS: Cleveland (1979)). The 1σ errors are calculated via the method in (Ferne, 1989; Kato et al., 2010). The robustness of the PDM results is confirmed by a variety of bootstraps. We made 100 samples, each containing 50% of the observations chosen at random, and performed the PDM analyses for each sample. The bootstrap results correspond to the 90% confidence intervals of θ statistics.

The $O - C$ diagram in Figure 2 shows the time difference of the superhump periods on each superhump cycle, and the linear and non-linear slopes represent the constant and varying periods, respectively. The positive linear slope before BJD 2,458,291.7 in ASASSN-18ey means that the period was constant and slightly longer than the assumed period during stage A (see also the top panel of Fig. 2a). The period suddenly dropped at BJD 2,458,291.7 and gradually increases during stage B. We first made a template profile from superhumps during BJD 2,458,279–2,458,405 (corresponds to 2018 June 9–2018 October 13) by folding them with the period estimated by PDM, and fitted superhumps at each cycle with the template to estimate the time of the superhump maxima (O). After that, the $O - C$ is calculated by subtracting the assumed fix period (C) \times the superhump cycle (E) from $O \times E$. The resultant times are given in Extended Data Table 2.

2 Overall optical behavior

We show all of our optical photometric data during the main outburst in Figure 5. The optical light curves show a complex behavior. They show a rapid rise at the onset of the outburst and a steep decay just after that. Then, radio flares were detected and actually sub-second optical flaring that is likely related to synchrotron emission was also discovered (Uttley et al., 2018; Gandhi et al., 2018; Tetarenko et al., 2018a; Russell et al., 2018; Trushkin et al., 2018). These nonthermal components would affect the optical light curves when stage A superhumps began to develop. The fast optical variability induced by synchrotron emission was observed commonly in the hard state among some of black-hole transients (Gandhi et al., 2008; Alfonso-Garzón et al., 2018). Actually the optical flux was scattered with respect to the X-ray flux especially in the hard state (Shidatsu et al., 2019), which cannot be predicted from the correlation between the optical and X-ray flux originating from the irradiated accretion disk (Russell et al., 2006).

The optical luminosity increased again since several days before the transition from stage A to stage B. Around that time, the radio activity was quenching, which was coincident with the hard-to-soft X-ray spectral transition (Tetarenko et al., 2018b; Broderick et al., 2018). The optical rise at the onset of the superhumps may be consistent with the sudden increase of the amount of angular momentum loss due to the tidal instability, and seem to resemble the light variations reproduced by numerical simulations in the past (Ichikawa et al., 1994).

3 SU UMa/WZ Sge-type stars and time evolution of their superhumps

Dwarf novae (DNe) are a subtype of cataclysmic variables (CVs) and are semi-detached binaries composed of a white dwarf (the primary) and a late-type main-sequence star (the secondary). There is an accretion disk around

¹<http://www.aavso.org/data-download/>

²<http://www.aavso.org/>

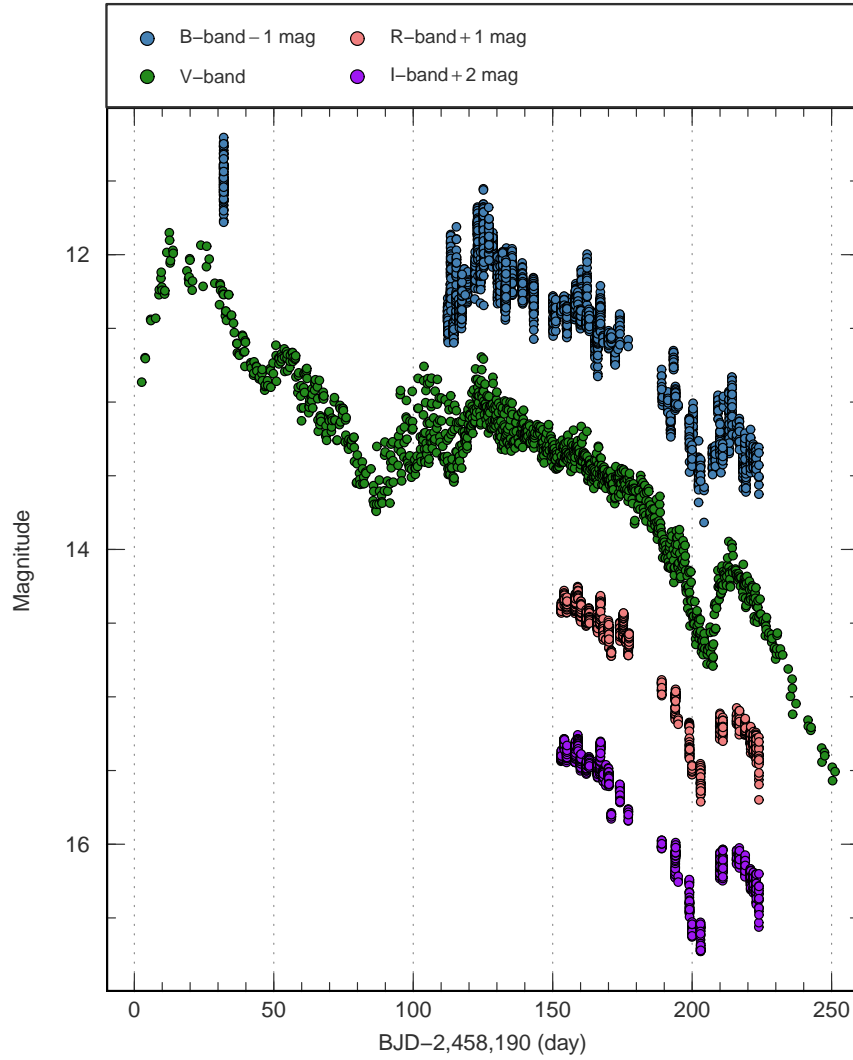


Figure 5: **Multi-color light curves of ASASSN-18ey.** The blue, green, pink, and purple points represent the light curves of B -band - 1mag, V -band, R -band + 1mag, and I -band + 2mag, respectively. The horizontal and vertical axis represent BJD-2,458,190 and Magnitude, respectively.

the primary. Because of the thermal-viscous instability in the disk, episodic abrupt increases of luminosity occur, which are called “outbursts” (Warner, 1995; Osaki, 1996).

SU UMa-type DNe are a subclass of DNe and show superoutbursts in addition to normal outbursts with amplitudes of 2–5 mag and several-days durations. Superoutbursts have ~ 6 -mag large amplitudes and ~ 2 -weeks long durations, and moreover, small-amplitude variations called “superhumps” with slightly longer periods than that of orbital humps. Superoutbursts and superhumps are believed to be the representation of the tidal instability (Whitehurst, 1988; Osaki, 1989). Superhumps can be classified into three stages as to variations of periods and amplitudes: stage A, stage B, and stage C. During stage A, the period is constant and the amplitude increases with time. During stage B, the period is varying and the amplitude gradually decreases. During stage C, the period is constant but shorter than the one during stage A, and the amplitude increases.

WZ Sge-type stars are an extreme subclass of DNe and belong to SU UMa-type DNe. Their mass accretion rate is extremely small, and hence, the frequency of outbursts is very low. The intervals between outbursts are typically larger than 5 years. The two main observational features characterizing WZ Sge-type stars are early superhumps and rebrightenings. Early superhumps are observed immediately after the superoutburst and their period is almost equal to the orbital one. Rebrightenings are sudden flux increases observed just after superoutbursts.

The period variation of superhumps is known to depend on the mass ratio of binary systems. Figure 6 shows the $O - C$ diagram of superhumps in three systems, ASASSN-16dt, WZ Sge, and SW UMa. Their mass ratios are 0.036(2), 0.078(3), and 0.100(3), respectively. The smaller the mass ratio is, the longer the stage A duration is and the shorter the stage C duration is (Kato, 2015).

The superhumps are excited by the strong tidal dissipation at the 3:1 resonance (Whitehurst, 1988). The accretion disk becomes elliptical, and then, the eccentric accretion disk precesses (Hirose, Osaki, 1990). The stage A superhumps are considered to represent the pure precession of the outermost ring of the accretion disk. The eccentricity wave propagates inwards with time and the pressure effect becomes significant. When the superhumps enter stage B and the superhump period is not determined only by the dynamical precession, since the pressure effect is not negligible (Kato, Osaki, 2013; Lubow, 1992; Hirose, Osaki, 1993; Montgomery, 2001).

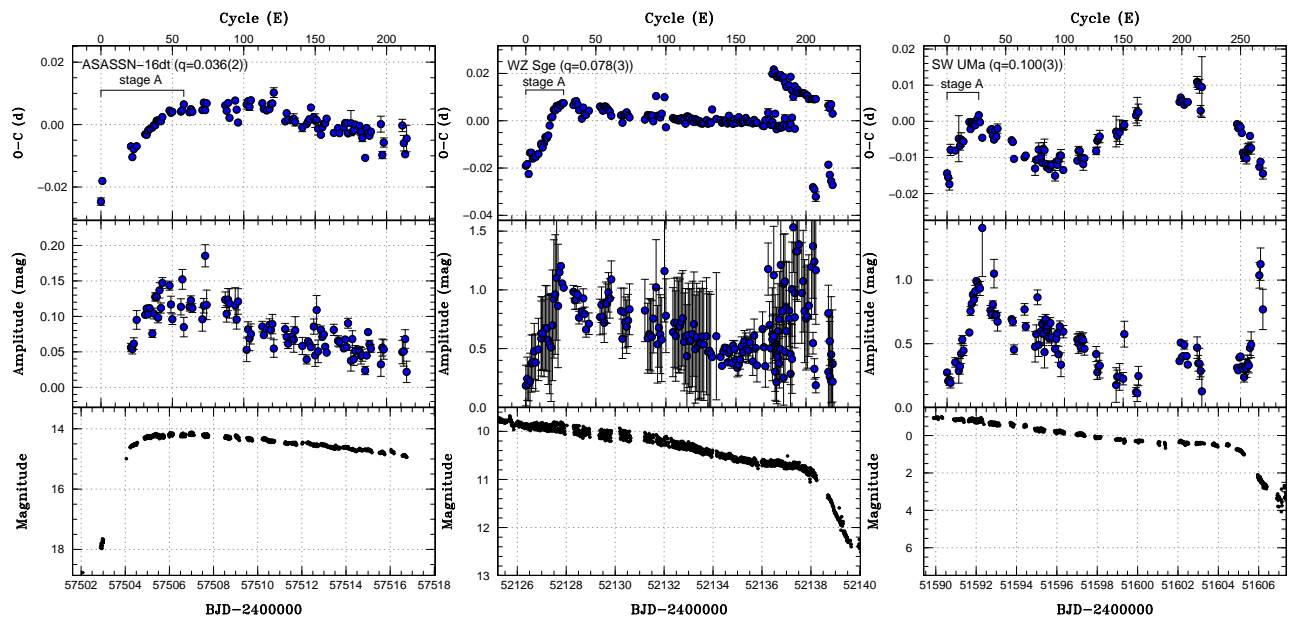


Figure 6: Typical period and amplitude variations of SU UMa-type stars during outburst. $O - C$ curves (upper panel), amplitudes of superhumps (middle panel) and light curves (lower panel) of SW UMa, WZ Sge and ASASSN-16dt. Each horizontal axis in units of BJD and cycle number is common to each of all column panels. The error bars represent 1σ statistic errors.

4 Estimation of black-hole masses with stage A superhumps

The method for estimating the binary mass ratio from the stage A superhump period and the orbital period has been developed in the study of SU UMa Sge-type stars. At the growing stage of superhumps (stage A), the superhumps are considered to represent the dynamical precession at the 3:1 resonance radius (Osaki, Kato, 2013). Here the growth time of superhumps is defined as the time until the eccentricity fully develops only at the 3:1 resonance radius. The fractional superhump excess ε^* is defined as, $\varepsilon^* \equiv 1 - P_{\text{orb}}/P_{\text{SH}}$, and ε^* of stage A superhumps is expressed by considering the dynamical precession as follows:

$$\varepsilon^* = \frac{q}{\sqrt{1+q}} \left[\frac{1}{4} \frac{1}{\sqrt{r}} b_{3/2}^{(1)} \right], \quad (1)$$

where r is the dimensionless radius normalized by the binary separation. Here, $b_{3/2}^{(1)}$ is the Laplace coefficient (Hirose, Osaki, 1990; Kato, Osaki, 2013). By substituting the 3:1 resonance radius, which is defined as $3^{(-2/3)}(1+q)^{-1/3}$, to equation (1), ε^* depends only on the binary mass ratio q (Kato, Osaki, 2013). We can estimate the binary mass ratio only by measurements of the orbital and stage A superhump periods.

In addition, we estimated the binary mass ratio in ASASSN-18ey only with the duration of stage A superhumps. Since superhumps are growing during stage A, the duration of stage A represents the growth time of the superhumps. In addition, it was predicted theoretically that the growth time of superhumps depends on q^{-2} (Lubow, 1991). The relation between q and the duration of stage A for WZ Sge-type objects was confirmed by using the observational data and the above method and Figure 3 shows the result (Kato, Osaki, 2013). This relation is independent of the nature of the primary star, and hence, applicable for black-hole binaries.

The mass-ratio estimation by the empirical relation between the stage B superhumps and the superhump excess (Patterson, 2001; Patterson et al., 2005) have used for a long time in many works including the very recent work (Torres et al., 2019). However, this method has some uncertainty because the periods of the stage B superhumps are variable as shown in Figure 6. Also, it is revealed that this method easily underestimate the binary mass ratio (Nakata et al., 2013). The method thus not suitable for the accurate estimation of black-hole masses.

5 Spectral energy distribution modelling

Figure 7 shows the multi-wavelength SEDs on July 8th (BJD 2,458,359) and August 19th (BJD 2,458,307) in 2018 when the source was simultaneously observed in the X-ray, ultraviolet (UV) and optical bands. The X-ray spectrum is extracted from simultaneous *Swift*/XRT data (ObsIDs 00010627076 and 00088657009) which were taken in the WT mode. The data are processed through the pipeline processing tool `xrtpipeline`. We select 1.0–10.0 keV XRT data. The UV flux is obtained from the *Swift*/UVOT images in the same ObsID as those of XRT through the standard tool `uvot2pha` provided by the *Swift* team. The optical flux is averaged per date.

We fit the multi-wavelength spectra with the model `phabs*redden*(optxrplir+bbbodyrad)`. The model `optxrplir` can simultaneously deal with the emission from an irradiated standard accretion disk and Comptonization component at the inner region. The hot corona which emits Comptonized photons is assumed to be located around the central object, and it extends to r_{corona} . The standard disk exists outside the hot corona and its outer part is reprocessed by X-rays emitted from the inner part of the disk and the corona. The models `phabs` and `redden` are implemented to correct interstellar absorption and extinction. The N_H is fixed to $1.5 \times 10^{21} \text{ cm}^{-2}$ (Uttley et al., 2018), and $E(B - V)$ is estimated to be 0.29 in fitting both of the two spectra. With the model `bbbodyrad`, we express the maximum contribution of the donor star to the optical flux, although it is less than 1% compared with the contribution from the outer accretion disk. We assume a K-type main-sequence star as a donor star with a temperature of 4,130 K, and that the donor star fills its Roche-lobe (Allen, 1973). According to Gaia data release 2, the distance to ASASSN-18ey is $3.06_{-0.82}^{+1.54}$ kpc (Gandhi et al., 2019). In addition, we fix kT_{pl} in `optxrplir` to 100 keV, since it is difficult to constrain the parameter without hard X-ray data. Although `optxrplir` can treat low-temperature Comptonization component, we do not add it. The black-hole mass is estimated to be $6.7 M_{\odot}$ in fitting simultaneously the two spectra, and we fix it to that value when fitting each spectrum separately. Then we assume the inclination angle is 60 deg.

The best-fit values of $\log(L/L_{\text{Edd}})$ and r_{corona} in units of R_g , $\log(R_{\text{out}}/R_g)$, and f_{out} are -0.70 , 13, 5.1, and 0.088 as for ObsID 00010627076, and -0.95 , 7, 5.1, and 0.14 as for ObsID 00088657009, respectively. Here, L_{Edd} is the Eddington luminosity, and R_g is the gravitational radius, respectively. The estimated disk radius is slightly

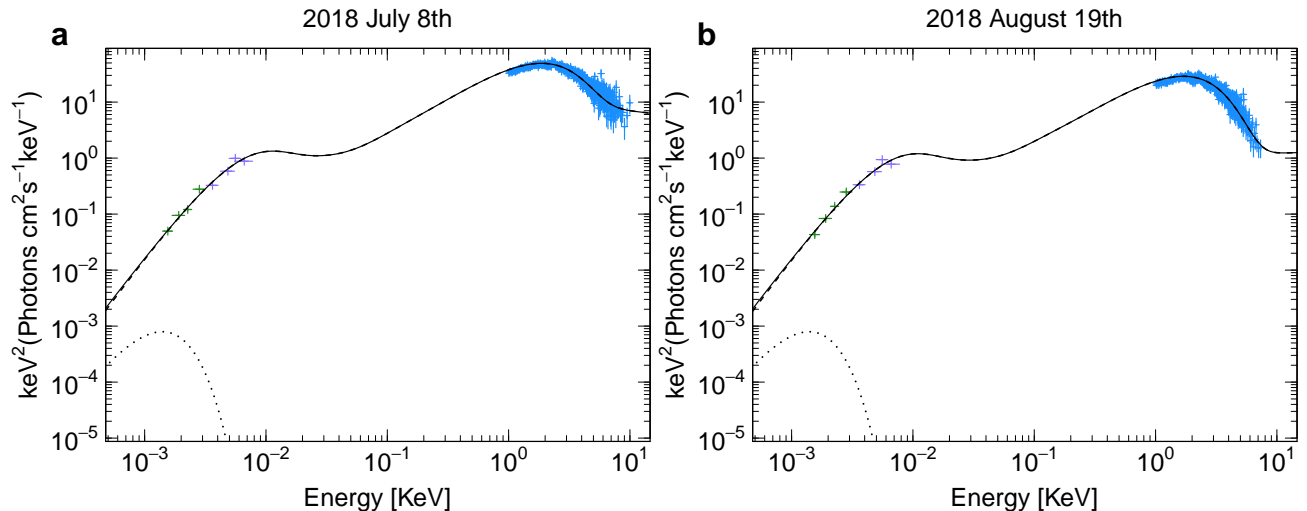


Figure 7: **Simultaneous, extinction-corrected multi-wavelength SEDs of ASASSN-18ey.** The broadband spectra on (a) BJD 2,458,307 (corresponds to 2018 July 7) and (b) BJD 2,458,349 (corresponds to 2018 August 18). The blue, purple, and green crosses show *Swift* XRT, *Swift* UVOT, and our optical data. The optical fluxes are averaged over the intervals, and the error bars represent their standard errors. The optical and *UV* flux are dereddened, and the X-ray flux are deabsorbed. The errors of X-ray and *UV* data represent 1σ confidence intervals. The dashed and dotted lines show the contribution of emissions from the irradiated disk with Comptonisation and from the companion star, respectively.

less than the 3:1 resonance radius, and appropriate as the disk radius after the onset of stage B superhumps (Ichikawa et al., 1993). The estimated f_{out} can be expected from the theoretical model of canonical irradiation on June 8th. Then the irradiated flux is more than 3–5 larger than the underlying disk flux expected from the standard temperature distribution. This means X-ray irradiation governs the emission from the outer disk.

The small-amplitude superhumps can be reproduced only by tidal dissipation as described in the main text. Although it is considered that the superhumps should not be reproduced only by the intrinsic luminosity of the viscous disk because of huge X-ray irradiation in black-hole binaries (Haswell et al., 2001), the actual irradiated flux in ASASSN-18ey was much smaller than expected in that study. Actually, the 14.9 *V*-band magnitude of the viscous disk on BJD 2,458,307 (corresponds to 2018 July 7) is comparable to the initial magnitude on the date of the discovery of this outburst, which means the temperature at the outer part of the underlying viscous disk is high enough to keep the hot state by itself. Although the origin of the superhump amplitudes in ASASSN-18ey, which are much larger than those of the past superhump candidates observed in other black-hole binaries (O’Donoghue, Charles, 1996; Uemura et al., 2002) is unclear, the hot surface area that is excited by tidal dissipation would be much larger because of the large disk expected from its long superhump period (see also Table 1), and the change in the vertical structure at the outer disk could be amplified via X-ray irradiation since X-ray irradiation makes the outer disk rim flared up (Cunningham, 1976).

6 Variations of color indices

We investigated the variations of color indices during BJD 2,458,302–2,458,310 (corresponds to 2018 July 2–2018 July 10), about a week after the onset of stage B superhumps. We estimated the $B - V$ and $V - R$ colors by approximating the simultaneous *V*-band magnitude to the *B* and *R* magnitudes with linear interpolation and averaged them with each of the stage A and stage B superhumps. The results are shown in Figure 8. Although a slight color change is observable as for dwarf novae during stage B superhumps (Neustroev et al., 2017), no appreciable color variations were detected in ASASSN-18ey during this time interval. The origin of color variations in dwarf novae is considered to be due to the enhanced viscous heating at the outer disk, and therefore, the color variation would not appear in black-hole binaries due to strong X-ray irradiation (Figure 7). Actually, our SED analyses suggest strong irradiation near this time period. In addition, no color variations in superhump candidates were confirmed also in GS 1124–68, another black-hole binary (Bailyn, 1992).

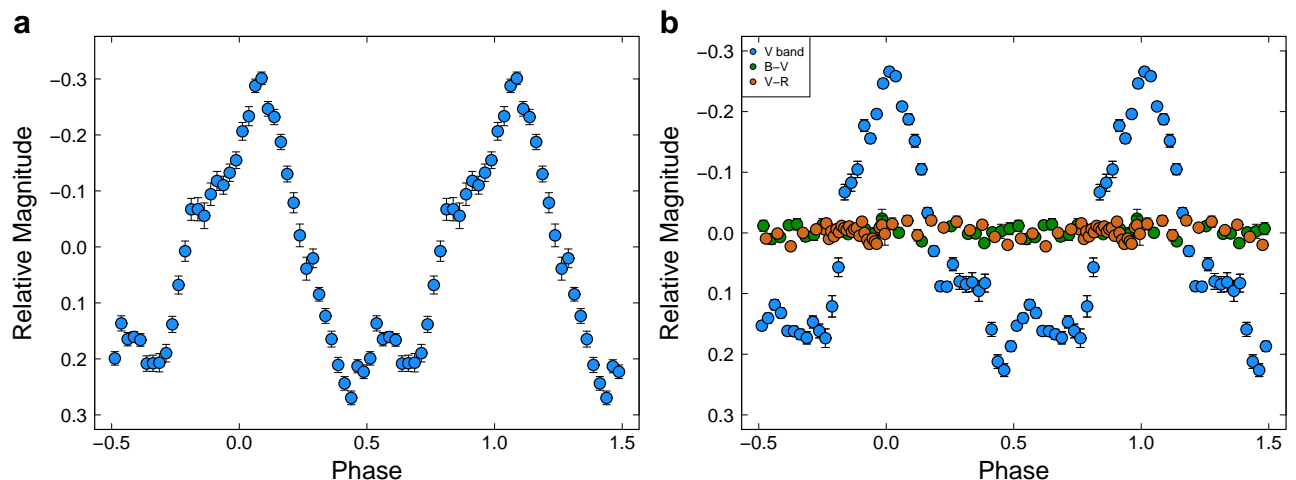


Figure 8: **Phase-averaged profiles of superhumps.** (a) Stage A superhump profile during BJD 2,458,279–2,458,295, and (b) stage B superhump profile during BJD 2,458,302–2,458,310. As for stage B superhumps, we focus on the time interval when the multi-color light curves are obtained in order to plot the $B - V$ and $V - R$ color variations together. The light curves are folded with the averaged period of each stage after subtracting the global trend of the light variations. The error bars represent 1σ statistic errors.

7 Black-hole binaries showing superhump candidates in the past

There are several transient black-hole binaries that have shown superhump candidates during outburst. However, the observational quality is not enough to surely confirm whether they are superhumps and the period variation characteristic to superhumps observed in SU UMa stars were not detected. We discuss each object in which superhump candidates were observed during outburst as follows and list these objects and their properties in Table 1.

The first suggestion that transient black-hole binaries may exhibit superhumps similar to those seen in SU UMa stars was made after the 1988 outburst in GS 2000+25 (QZ Vul) (Charles et al., 1991). They argued that the observed hump profile was not caused by ellipsoidal variations. Additionally, X-ray heating of the donor star was ruled out because no color variations were observed in these humps. Moreover, geometrical effects of the outer accretion disk were also excluded because of the expected low inclination. However, the number of data points were less than several hundred, and they did not demonstrate they are clearly superhumps (Charles et al., 1991). After that work, the orbital period was measured by other authors (Chevalier, Ilovaisky, 1993), which proved the estimated superhump period was slightly longer than the orbital period (O’Donoghue, Charles, 1996).

In the 1991 outburst of GS 1124–68, similar humps to those observed in GS 2000+25 with a period slightly longer than the orbital period were found (Bailyn, 1992), and then, they were suggested to be superhumps as discussed in GS 2000+25 (Charles et al., 1991). However, the coverage of the data is sparse and the total length of the observations was only a few days during the outburst which typically continues for more than 100 days. The data were reanalyzed after their work, and the period of these humps were estimated to be shorter (O’Donoghue, Charles, 1996). Since the data quality is thus not at all convincing, it is difficult to distinguish the superhump period that they argued from the orbital period measured by other authors (Remillard et al., 1992).

Two types of optical variability were discovered in GRO J0422+32 (V518 Per), another black-hole binary, during its 1992–1993 outburst. The observed dip-type variations with a shorter period and another kind of variations with a longer period were considered to be the orbital modulations and superhumps, respectively (Kato et al., 1995). The data used in this paper had been the densest one among the data taken in the above three systems prior to our work, and they succeeded to estimate the superhump period within a 0.5% accuracy. They noticed the hump period changed with time during outburst, but did not confirm if this feature originated from the actual period change of superhumps, and interpreted the period decrease as being due to the appearance of the orbital modulations. Soon after that work, the hump periods at the late stage of the outburst and in quiescence were estimated by (Chevalier, Ilovaisky, 1995), and they were identical with each other. The authors hence regard them as orbital modulations. Also, the periods were comparable to the hump period at the latter

Table 1: Objects Showing Superhumps during Outburst in Black-Hole Binaries.

Object Name	Orbital Period [d]	Superhump Period [d]	$M_1 [M_\odot]$	Donor*	$q = M_2/M_1$
GS 2000+25 (QZ Vul)	0.344098(5) ^[1]	0.3474(3) ^[2]	8.5(1.5) ^[3]	K3-6/5 ^[4]	0.03-0.25 ^[3]
GS 1124-68 (Nova Musca)	0.4333(6) ^[5]	0.4376(10) ^[2]	6.95(60) ^[6]	K3-4/5 ^[7]	0.09-0.17 ^[6]
GRO J0422-32 (V518 Per)	0.2121600(2) ^[8]	0.2157(12) ^[2]	3.57(34) ^[9]	M0-2/5 ^[9]	0.1093(86) ^[9]
XTE J1118+480 (KV UMa)	0.169930(4) ^[10,11]	0.170529(6) ^[12]	6.0-7.7 ^[11]	K5/5 ^[13]	0.05 ^[14]
GRS 1716-249 (V2293 Oph)	-	0.6127 ^[15]	>4.9 ^[15]	M0-5/5 ^[16]	-
GRS 1009-45 (MM Vel)	0.285206(14) ^[17]	0.1996 ^[18]	4.4 ^[17]	K7-M0/5 ^[17]	7.3(0.8) ^[17]
XTE J1859+226 (V406 Vul)	0.274(2) ^[19]	0.38385(73) ^[20]	>5.4 ^[19]	G5 ^[21]	-
MAXI J1820+070 (ASASSN-18ey)	-	0.688907(9)	-	-	~0.1

* Spectral type.

References: [1] Chevalier, Ilovaisky (1993), [2] O'Donoghue, Charles (1996), [3] Orosz (2003), [4] Harlaftis et al. (1996), [5] Remillard et al. (1992), [6] Gelino et al. (2001), [7] Casares et al. (1997), [8] Webb et al. (2000), [9] Gelino, Harrison (2003), [10] Wagner et al. (2001), [11] McClintock et al. (2001a), [12] Uemura et al. (2002), [13] Gelino et al. (2006), [14] González Hernández et al. (2014), [15] Masetti et al. (1996), [16] Chaty et al. (2002), [17] Filippenko et al. (1999), [18] Masetti et al. (1997), [19] Corral-Santana et al. (2011), [20] Uemura et al. (2004), [21] Filippenko, Chornock (2001)

stage of the outburst in (Kato et al., 1995).

Several years later, XTE J1118+480 (KV UMa), a newly discovered X-ray transient, showed during its 2000 outburst optical modulations having periods slightly longer than the orbital period (Uemura et al., 2002; Wagner et al., 2001; McClintock et al., 2001b). The hump period was estimated within the 0.05% accuracy, and thus, they clearly detected the existence of superhumps during outburst for the first time by using their extensive data. Since the hump profile was not easily explained by the orbital periods, the detected continuous period decreases strongly suggested the variations are superhumps. In this object, the period variations of superhump candidates were detected for the first time among black-hole binaries. However, the authors were not able to classify the superhumps into each stage, so the certain detection of humps quite similar to those observed in SU UMa stars was not completed. This is because they did not obtain the data of the initial stage of superhumps, and because the detailed definition of the stages of superhumps was established in 2009 (Kato et al., 2009) even in SU UMa stars. Also, this system is not classical because it did not enter the canonical spectral state evolution of outbursts in comparison with many other black-hole transients (Tanaka, Shibazaki, 1996; Chen et al., 1997). Therefore our study is the first one showing the absolute discovery of superhumps in normal transient black-hole X-ray binaries. In addition, the superhump modulations were also confirmed in the rebrightenings in 2005 (Zurita et al., 2006).

Although the observational data were sparse due to the dimness of the outbursts, there are three other objects possibly showing superhumps during outburst. It is unclear because of their unknown orbital periods, but it was argued that superhump-like modulations were found in GRS 1716-249 and GRS 1009-45 during outburst (Masetti et al., 1996, 1997). Additionally, coherent optical variations appeared in XTE J1859+226, which have possibly a longer period than the orbital one (Zurita et al., 2002; Uemura et al., 2004), though the period is much longer than the orbital period lately measured by the optical photometry of ellipsoidal modulations in quiescence (Corral-Santana et al., 2011).

As described above, it is not rare that superhumps are observed during outburst in black-hole binaries. The most plausible model of the origin of superhumps is the precession of the eccentric disk exerted by the tidal instability, which is triggered in small mass-ratio binary systems. The condition is considered to be $q \lesssim 0.25$ (Whitehurst, 1988; Osaki, 1989; Osaki, Meyer, 2002). Generally, most of the black-hole low-mass X-ray binaries would satisfy this condition. However, the optical outbursts in this kind of objects are usually dim due to their distance, and hence, this may have prevented universal detections of superhumps in black hole X-ray binaries. Nevertheless, the current development of optical telescopes and observational networks will enable us to detect

superhumps in many transient black-hole binaries.

References

- Alfonso-Garzón, J., et al. 2018, *Astron. Astrophys.*, 620, A110
- Allen, C. W. 1973, *Astrophysical quantities* (London: University of London, Athlone Press)
- Atri, P., et al. 2020, *Mon. Not. R. Astron. Soc.*, 493, L81
- Baglio, M. C., Russell, D. M., & Lewis, F. 2018, *The Astronomer's Telegram*, 11418
- Bailyn, C. D. 1992, *Astrophys. J.*, 391, 298
- Broderick, J., Russell, T., Bright, J., Rowlinson, A., Fender, R., & Done, C. 2018, *The Astronomer's Telegram*, 11887
- Casares, J., Martin, E. L., Charles, P. A., Molaro, P., & Rebolo, R. 1997, *New Astron.*, 1, 299
- Charles, P. A., Kidger, M. R., Pavlenko, E. P., Prokof'eva, V. V., & Callanan, P. J. 1991, *Mon. Not. R. Astron. Soc.*, 249, 567
- Chaty, S., Mirabel, I. F., Goldoni, P., Mereghetti, S., Duc, P.-A., Martí, J., & Mignani, R. P. 2002, *Mon. Not. R. Astron. Soc.*, 331, 1065
- Chen, W., Shrader, C. R., & Livio, M. 1997, *Astrophys. J.*, 491, 312
- Chevalier, C., & Ilovaisky, S. A. 1993, *Astron. Astrophys.*, 269, 301
- Chevalier, C., & Ilovaisky, S. A. 1995, *Astron. Astrophys.*, 297, 103
- Cleveland, W. S. 1979, *J. Amer. Statist. Assoc.*, 74, 829
- Corral-Santana, J. M., Casares, J., Shahbaz, T., Zurita, C., Martínez-Pais, I. G., & Rodríguez-Gil, P. 2011, *Mon. Not. R. Astron. Soc.*, 413, L15
- Cunningham, C. 1976, *Astrophys. J.*, 208, 534
- Denisenko, D. 2018, *The Astronomer's Telegram*, 11400
- Done, C., Gierliński, M., & Kubota, A. 2007, *Astron. Astrophys. Rev.*, 15, 1
- Dunn, R. J. H., Fender, R. P., Körding, E. G., Cabanac, C., & Belloni, T. 2008, *Mon. Not. R. Astron. Soc.*, 387, 545
- Esin, A. A., McClintock, J. E., & Narayan, R. 1997, *Astrophys. J.*, 489, 865
- Fernie, J. D. 1989, *Publ. Astron. Soc. Pac.*, 101, 225
- Filippenko, A. V., & Chornock, R. 2001, *IAU Circ.*, 7644
- Filippenko, A. V., Leonard, D. C., Matheson, T., Li, W., Moran, E. C., & Riess, A. G. 1999, *Publ. Astron. Soc. Pac.*, 111, 969
- Frank, J., King, A., & Raine, D. J. 2002, *Accretion Power in Astrophysics: Third Edition* (Cambridge: Cambridge University Press)
- Gandhi, P., et al. 2008, *Mon. Not. R. Astron. Soc.*, 390, L29
- Gandhi, P., Paice, J. A., Littlefair, S. P., Dhillon, V. S., Chote, P., & Marsh, T. R. 2018, *The Astronomer's Telegram*, 11437
- Gandhi, Poshak, Rao, Anjali, Johnson, Michael A. C., Paice, John A., & Maccarone, Thomas J. 2019, *Mon. Not. R. Astron. Soc.*, 485, 2642

- Gelino, D. M., Balman, Ş., Kızıloğlu, Ü., Yılmaz, A., Kalemci, E., & Tomsick, J. A. 2006, *Astrophys. J.*, 642, 438
- Gelino, D. M., & Harrison, T. E. 2003, *Astrophys. J.*, 599, 1254
- Gelino, D. M., Harrison, T. E., & McNamara, B. J. 2001, *Astron. J.*, 122, 971
- González Hernández, J. I., Rebolo, R., & Casares, J. 2014, *Mon. Not. R. Astron. Soc.*, 438, L21
- Harlaftis, E. T., Horne, K., & Filippenko, A. V. 1996, *Publ. Astron. Soc. Pac.*, 108, 762
- Haswell, C. A., King, A. R., Murray, J. R., & Charles, P. A. 2001, *Mon. Not. R. Astron. Soc.*, 321, 475
- Henden, A. A., Templeton, M., Terrell, D., Smith, T. C., Levine, S., & Welch, D. 2016, *VizieR Online Data Catalog*, 2336
- Hirose, M., & Osaki, Y. 1990, *Publ. Astron. Soc. Jpn.*, 42, 135
- Hirose, M., & Osaki, Y. 1993, *Publ. Astron. Soc. Jpn.*, 45, 595
- Ichikawa, S., Hirose, M., & Osaki, Y. 1993, *Publ. Astron. Soc. Jpn.*, 45, 243
- Ichikawa, S., Mineshige, S., & Kato, T. 1994, *Astrophys. J.*, 435, 748
- Kara, E., et al. 2019, *Nature*, 565, 198
- Kato, T. 2015, *Publ. Astron. Soc. Jpn.*, 67, 108
- Kato, T., et al. 2009, *Publ. Astron. Soc. Jpn.*, 61, S395
- Kato, T., et al. 2012, *Publ. Astron. Soc. Jpn.*, 64, 21
- Kato, T., et al. 2010, *Publ. Astron. Soc. Jpn.*, 62, 1525
- Kato, T., Mineshige, S., & Hirata, R. 1995, *Publ. Astron. Soc. Jpn.*, 47, 31
- Kato, T., & Osaki, Y. 2013, *Publ. Astron. Soc. Jpn.*, 65, 115
- Kato, T., & Uemura, M. 2012, *Publ. Astron. Soc. Jpn.*, 64, 122
- Kato, T., Uemura, M., Ishioka, R., Nogami, D., Kunjaya, C., Baba, H., & Yamaoka, H. 2004, *Publ. Astron. Soc. Jpn.*, 56, S1
- Kawamuro, T., et al. 2018, *The Astronomer's Telegram*, 11399
- Kuulkers, E., Howell, S. B., & van Paradijs, J. 1996, *Astrophys. J.*, 462, L87
- Lubow, S. H. 1991, *Astrophys. J.*, 381, 268
- Lubow, S. H. 1992, *Astrophys. J.*, 401, 317
- McClintock, J., Garcia, M., Caldwell, N., Falco, E. E., Garnavich, P. M., & Zhao, P. 2001a, *Astrophys. J.*, 551, L147
- McClintock, J. E., et al. 2001b, *Astrophys. J.*, 555, 477
- Masetti, N., Bianchini, A., Bonibaker, J., della Valle, M., & Vio, R. 1996, *Astron. Astrophys.*, 314, 123
- Masetti, N., Bianchini, A., & della Valle, M. 1997, *Astron. Astrophys.*, 317, 769
- Meyer, F. 1984, *Astron. Astrophys.*, 131, 303
- Montgomery, M. M. 2001, *Mon. Not. R. Astron. Soc.*, 325, 761
- Nakata, C., et al. 2013, *Publ. Astron. Soc. Jpn.*, 65, 117
- Narayan, R., & Yi, I. 1994, *Astrophys. J.*, 428, L13

- Neustroev, V. V., et al. 2017, *Mon. Not. R. Astron. Soc.*, 467, 597
- Neustroev, V. V., et al. 2018, *Astron. Astrophys.*, 611, A13
- O'Donoghue, D., & Charles, P. A. 1996, *Mon. Not. R. Astron. Soc.*, 282, 191
- Orosz, J. A. 2003, in van der Hucht K., Herrero A., Esteban C., eds, *IAU Symposium Vol. 212, A Massive Star Odyssey: From Main Sequence to Supernova*. p. 365
- Osaki, Y. 1989, *Publ. Astron. Soc. Jpn.*, 41, 1005
- Osaki, Y. 1996, *Publ. Astron. Soc. Pac.*, 108, 39
- Osaki, Y., & Kato, T. 2013, *Publ. Astron. Soc. Jpn.*, 65, 50
- Osaki, Y., & Meyer, F. 2002, *Astron. Astrophys.*, 383, 574
- Patterson, J. 2001, *Publ. Astron. Soc. Pac.*, 113, 736
- Patterson, J., et al. 2005, *Publ. Astron. Soc. Pac.*, 117, 1204
- Remillard, R. A., McClintock, J. E., & Bailyn, C. D. 1992, *Astrophys. J.*, 399, L145
- Remillard, R. A., & McClintock, J. E. 2006, *Annu. Rev. Astron. Astr.*, 44, 49
- Russell, D. M., et al. 2018, *The Astronomer's Telegram*, 11533
- Russell, D. M., Fender, R. P., Hynes, R. I., Brocksopp, C., Homan, J., Jonker, P. G., & Buxton, M. M. 2006, *Mon. Not. R. Astron. Soc.*, 371, 1334
- Shidatsu, M., et al. 2018, *Astrophys. J.*, 868, 54
- Shidatsu, Megumi, Nakahira, Satoshi, Murata, Katsuhiro L., Adachi, Ryo, Kawai, Nobuyuki, Ueda, Yoshihiro, & Negoro, Hitoshi 2019, *ApJ*, 874, 183
- Stellingwerf, R. F. 1978, *Astrophys. J.*, 224, 953
- Tanaka, Y., & Shibazaki, N. 1996, *Annu. Rev. Astron. Astr.*, 34, 607
- Tetarenko, A. J., Bremer, M., Bright, J., Sivakoff, G. R., Miller-Jones, J. C. A., Russell, T. D., & Japote Xrb Collaboration 2018a, *The Astronomer's Telegram*, 11440
- Tetarenko, A. J., Petitpas, G., Sivakoff, G. R., Miller-Jones, J. C. A., Russell, T. D., Schieven, G., & Japote Xrb Collaboration 2018b, *The Astronomer's Telegram*, 11831
- Torres, M. A. P., Casares, J., Jiménez-Ibarra, F., Álvarez-Hernández, A., Muñoz-Darias, T., Armas Padilla, M., Jonker, P. G., & Heida, M. 2020, *Astrophys. J.*, 893, L37
- Torres, M. A. P., Casares, J., Jiménez-Ibarra, F., Muñoz-Darias, T., Armas Padilla, M., Jonker, P. G., & Heida, M. 2019, *ApJ*, 882, L21
- Trushkin, S. A., Nizhelskij, N. A., Tsybulev, P. G., & Erkenov, A. 2018, *The Astronomer's Telegram*, 11539
- Tucker, M. A., et al. 2018, *Astrophys. J.*, 867, L9
- Uemura, M., et al. 2002, *Publ. Astron. Soc. Jpn.*, 54, 285
- Uemura, M., Kato, T., Pavlenko, E., Shugarov, S., Mitskevich, M., Fried, R. E., & Sano, Y. 2004, *Publ. Astron. Soc. Jpn.*, 56, S147
- Uttley, P., et al. 2018, *The Astronomer's Telegram*, 11423
- Wagner, R. M., Foltz, C. B., Shahbaz, T., Casares, J., Charles, P. A., Starrfield, S. G., & Hewett, P. 2001, *Astrophys. J.*, 556, 42
- Warner, B. 1995, *Cataclysmic Variable Stars* (Cambridge: Cambridge University Press)

- Webb, N. A., Naylor, T., Ioannou, Z., Charles, P. A., & Shahbaz, T. 2000, *Mon. Not. R. Astron. Soc.*, 317, 528
- Whitehurst, R. 1988, *Mon. Not. R. Astron. Soc.*, 232, 35
- Zurita, C., et al. 2002, *Mon. Not. R. Astron. Soc.*, 334, 999
- Zurita, C., et al. 2006, *Astrophys. J.*, 644, 432

Extended Data tables

Table E.1: Log of observations of the 2018 outburst in ASASSN-18ey.

Start*	End*	Mag [†]	Error [‡]	N [§]	Obs
58192.8343	58192.9583	12.945	0.002	3230	LCO
58193.8548	58193.9223	12.761	0.002	1758	LCO
58195.7754	58195.8155	12.565	0.009	206	HaC
58195.8259	58195.9040	12.500	0.002	1895	LCO
58196.8272	58196.8776	12.539	0.007	261	HaC
58197.5629	58197.6761	12.513	0.005	293	BSM
58197.8165	58197.8803	12.471	0.004	320	HaC
58198.8138	58198.8811	12.406	0.005	340	HaC
58198.8239	58198.9026	12.277	0.005	206	LMA
58199.5374	58199.6521	1.291	0.004	596	Vih
58199.6115	58199.6602	2.187	0.005	588	Vih
58199.8052	58199.9449	12.287	0.002	3649	LCO
58199.8103	58199.8812	12.343	0.005	361	HaC
58200.8169	58200.9614	12.318	0.005	252	UJH
58201.5912	58201.6351	2.071	0.005	487	Vih
58201.5935	58201.6357	1.137	0.006	511	Vih
58201.8165	58201.9339	12.130	0.005	280	RIT
58201.8295	58201.9324	12.147	0.024	10	RIT
58202.5830	58202.5981	12.074	0.008	84	Trt
58202.5890	58202.6099	1.048	0.010	165	Vih
58202.8141	58202.9206	12.035	0.004	562	RIT
58202.8142	58202.9201	12.056	0.011	68	RIT
58202.8187	58202.9568	12.113	0.006	325	UJH
58202.8204	58202.8611	12.114	0.004	605	LCO
58203.5108	58203.5388	-0.408	0.013	18	CRI
58203.5116	58203.5441	0.423	0.011	21	CRI
58203.8014	58203.8790	12.070	0.004	453	HaC
58203.8016	58203.9212	11.954	0.002	1270	RIT
58203.8105	58203.8861	11.977	0.005	188	LMA
58203.8200	58203.9578	12.048	0.006	344	UJH
58204.7963	58204.8797	12.176	0.004	377	HaC
58205.8310	58205.8833	12.119	0.004	462	HaC
58206.7987	58206.8884	12.105	0.005	295	HaC
58207.5319	58207.5995	-0.598	0.009	43	CRI
58207.5346	58207.5987	0.495	0.008	43	CRI
58207.7879	58207.8805	12.042	0.003	804	HaC
58208.7848	58208.9195	12.086	0.003	1281	RIT
58208.7851	58208.8805	12.234	0.003	809	HaC
58208.8205	58208.8721	12.181	0.014	125	UJH

Table E.1: Log of observations of the 2018 outburst in ASASSN-18ey (continued).

Start*	End*	Mag [†]	Error [‡]	N [§]	Obs
58208.9486	58209.0466	12.083	0.007	134	SGE
58209.4513	58209.6169	12.088	0.004	188	OAR
58209.7823	58209.8812	12.251	0.003	837	HaC
58209.8194	58209.9373	12.078	0.005	269	UJH
58209.8862	58209.9326	12.256	0.007	90	BJA
58209.9487	58210.0212	12.158	0.005	250	SGE
58210.7795	58210.8811	12.298	0.003	875	HaC
58210.7883	58210.8692	12.239	0.003	1078	LCO
58210.8184	58210.8853	12.241	0.012	166	UJH
58210.8333	58210.9164	12.123	0.003	873	RIT
58210.9282	58211.0167	12.137	0.004	300	SGE
58211.5225	58211.6561	12.281	0.003	554	BSM
58211.7769	58211.8812	12.230	0.003	868	HaC
58212.5061	58212.5950	-0.427	0.006	182	CRI
58212.5065	58212.5952	0.582	0.007	181	CRI
58212.7748	58212.8818	12.284	0.003	904	HaC
58212.9509	58213.0222	12.140	0.006	167	SGE
58213.5143	58213.5841	-0.384	0.005	145	CRI
58213.5145	58213.5843	0.579	0.008	145	CRI
58213.5736	58213.6044	12.155	0.005	170	Trt
58213.7720	58213.8847	12.192	0.003	949	HaC
58213.8505	58213.8853	11.997	0.009	67	UJH
58214.4895	58214.5943	-0.466	0.004	283	CRI
58214.4897	58214.5941	0.496	0.005	282	CRI
58214.7692	58214.8816	12.176	0.002	937	HaC
58215.4928	58215.6032	-0.411	0.004	299	CRI
58215.4930	58215.6034	0.642	0.005	300	CRI
58215.7665	58215.8853	12.169	0.003	983	HaC
58215.7749	58215.8089	12.003	0.007	158	RIT
58215.8178	58215.8855	12.166	0.007	170	UJH
58215.8472	58215.9341	12.157	0.006	163	BJA
58216.4295	58216.4965	0.601	0.004	410	CRI
58216.7636	58216.8854	12.148	0.002	1024	HaC
58216.8181	58216.8852	12.117	0.007	160	UJH
58216.8267	58216.8511	12.119	0.009	47	BJA
58217.7609	58217.8861	12.207	0.003	1056	HaC
58218.7581	58218.8832	12.340	0.003	1041	HaC
58218.8194	58218.8853	12.260	0.009	167	UJH
58219.0011	58219.0053	12.105	0.025	14	SGE
58219.5188	58219.5927	12.227	0.003	399	Trt
58219.7521	58219.9086	12.146	0.002	1495	RIT
58219.7894	58219.8861	12.266	0.003	812	HaC
58220.4988	58220.5835	12.252	0.005	201	OAR
58220.5586	58220.6416	12.475	0.002	3760	Trt
58220.7511	58220.8931	12.163	0.002	1544	RIT
58220.7867	58220.8249	12.192	0.007	139	HaC
58220.7868	58220.8868	11.681	0.004	859	HaC
58220.8714	58220.9267	12.263	0.006	314	HBB
58221.1919	58221.2992	12.536	0.003	897	MGW
58221.5480	58221.6597	12.585	0.006	288	Van
58221.5483	58221.6596	12.569	0.004	616	Van
58221.7348	58221.8569	12.286	0.004	730	HBB

Table E.1: Log of observations of the 2018 outburst in ASASSN-18ey (continued).

Start*	End*	Mag [†]	Error [‡]	N [§]	Obs
58221.7839	58221.8867	12.268	0.002	1212	HaC
58221.9131	58221.9545	12.582	0.005	253	COO
58221.9501	58221.9707	12.618	0.007	196	LPA
58221.9721	58221.9954	11.759	0.011	199	LPA
58221.9972	58222.0187	12.250	0.007	198	LPA
58222.0201	58222.0316	12.451	0.015	71	LPA
58222.5303	58222.6026	12.717	0.002	4035	Trt
58222.7811	58222.8839	12.387	0.003	1214	HaC
58222.9539	58222.9764	12.593	0.008	200	LPA
58222.9780	58223.0010	11.722	0.019	141	LPA
58223.0024	58223.0340	12.425	0.006	240	LPA
58223.7783	58223.8875	12.274	0.002	1284	HaC
58224.7755	58224.8847	12.415	0.003	1274	HaC
58225.5092	58225.6596	12.860	0.003	1225	Van
58225.8117	58225.8847	12.533	0.003	892	HaC
58226.5173	58226.6597	12.877	0.003	1143	Van
58226.7803	58226.8751	12.641	0.007	228	UJH
58226.8089	58226.8882	12.611	0.003	921	HaC
58226.9493	58227.0178	12.531	0.004	176	SGE
58227.5257	58227.6597	12.937	0.003	1056	Van
58227.5552	58227.6823	12.858	0.002	1108	deM
58227.5646	58227.6780	12.562	0.002	683	IMi
58227.9954	58227.9988	12.538	0.028	13	SGE
58228.5437	58228.6597	12.865	0.003	742	Van
58228.7786	58228.8748	12.601	0.006	226	UJH
58228.8001	58228.9164	12.734	0.004	337	BJA
58228.8764	58228.9976	12.520	0.003	420	SGE
58229.5014	58229.6525	13.043	0.003	876	Van
58229.7774	58229.8264	12.652	0.018	96	UJH
58229.7804	58229.8946	12.543	0.002	1292	RIT
58229.7943	58229.8013	12.578	0.008	73	RIT
58229.9881	58230.0027	12.621	0.009	54	SGE
58230.4815	58230.6394	12.756	0.003	526	BSM
58230.7623	58230.8964	12.675	0.002	1496	RIT
58230.9369	58230.9958	12.637	0.004	220	SGE
58231.5254	58231.6384	12.878	0.003	386	BSM
58231.7568	58231.8888	12.748	0.003	1496	HaC
58231.8831	58231.9974	12.723	0.003	346	SGE
58232.7540	58232.8887	12.810	0.006	191	HaC
58232.7997	58232.9131	12.954	0.003	329	BJA
58232.9036	58233.0010	12.766	0.006	444	SGE
58233.5033	58233.6310	12.854	0.003	441	BSM
58233.7512	58233.8893	12.766	0.007	194	HaC
58233.9020	58233.9952	12.684	0.004	251	SGE
58234.4837	58234.5321	13.007	0.002	2387	Trt
58234.7767	58234.8751	12.879	0.006	245	UJH
58234.7996	58234.8603	13.000	0.006	177	BJA
58235.7686	58235.8406	12.843	0.017	88	UJH
58236.7429	58236.8899	12.906	0.006	208	HaC
58236.8886	58236.9769	12.813	0.003	450	SGE
58237.7401	58237.8869	12.878	0.006	207	HaC
58237.7776	58237.8748	12.934	0.006	238	UJH

Table E.1: Log of observations of the 2018 outburst in ASASSN-18ey (continued).

Start*	End*	Mag [†]	Error [‡]	N [§]	Obs
58237.8006	58237.9131	13.068	0.003	326	BJA
58237.8609	58237.9618	12.864	0.003	424	SGE
58238.7551	58238.8896	12.789	0.006	193	HaC
58238.7768	58238.8752	12.833	0.006	235	UJH
58238.8098	58238.8739	12.747	0.004	254	RIT
58239.4609	58239.6014	12.845	0.003	505	BSM
58239.7352	58239.8867	12.786	0.006	109	HaC
58239.7367	58239.8798	12.758	0.002	1625	RIT
58239.7834	58239.8751	12.848	0.019	50	UJH
58239.8761	58239.8889	12.765	0.007	74	SGE
58240.7324	58240.8873	12.664	0.007	112	HaC
58240.7401	58240.8842	12.620	0.002	1614	RIT
58241.7297	58241.8898	12.726	0.005	116	HaC
58241.8438	58241.9365	12.685	0.003	406	SGE
58242.4846	58242.5463	12.896	0.003	1694	Trt
58242.5028	58242.5463	12.833	0.003	695	Trt
58242.7268	58242.8907	12.687	0.004	119	HaC
58243.4229	58243.5802	12.722	0.003	407	BSM
58243.7006	58243.8739	12.604	0.002	1876	RIT
58243.7241	58243.8910	12.683	0.007	120	HaC
58243.7686	58243.8270	12.848	0.003	153	BJA
58243.7790	58243.8748	12.737	0.006	231	UJH
58243.8745	58243.9554	12.741	0.002	449	SGE
58244.4692	58244.5708	12.807	0.001	3466	Trt
58244.7212	58244.8950	12.696	0.005	127	HaC
58244.7356	58244.8751	12.732	0.005	330	UJH
58244.8546	58244.9561	12.682	0.005	153	SGE
58245.1125	58245.3263	12.731	0.001	1647	MGW
58245.4270	58245.6267	12.827	0.002	604	BSM
58245.4656	58245.5808	12.836	0.001	3929	Trt
58245.4809	58245.6804	12.985	0.003	805	Van
58245.4833	58245.6773	12.994	0.010	70	Van
58245.7186	58245.8920	12.764	0.005	126	HaC
58245.7412	58245.8752	12.780	0.010	259	UJH
58246.4322	58246.6262	12.796	0.002	588	BSM
58246.4628	58246.5825	12.805	0.001	4084	Trt
58246.5569	58246.6363	12.671	0.002	170	RJW
58246.6334	58246.8950	12.688	0.004	193	HaC
58246.6758	58246.8744	12.655	0.001	2193	RIT
58246.7402	58246.8740	12.752	0.005	316	UJH
58246.8466	58246.9709	12.660	0.001	800	SGE
58247.2476	58247.3264	12.777	0.002	616	MGW
58247.4602	58247.5632	12.782	0.002	1996	Trt
58247.4775	58247.6733	12.986	0.004	246	Van
58247.5406	58247.6286	12.712	0.002	224	RJW
58247.6479	58247.8923	12.702	0.008	118	HaC
58247.6880	58247.8728	12.687	0.001	2137	RIT
58247.9145	58247.9782	12.786	0.002	400	SGE
58248.6281	58248.8929	12.878	0.005	194	HaC
58248.8559	58248.9448	12.784	0.002	568	SGE
58249.4382	58249.6733	13.134	0.002	492	Van
58249.5074	58249.6273	13.184	0.002	422	CDZ

Table E.1: Log of observations of the 2018 outburst in ASASSN-18ey (continued).

Start*	End*	Mag [†]	Error [‡]	N [§]	Obs
58249.5178	58249.6025	12.879	0.002	215	RJW
58249.6250	58249.8895	12.975	0.007	195	HaC
58249.7702	58249.7899	12.915	0.010	67	LPA
58249.9000	58249.9792	13.055	0.002	213	SGE
58250.4588	58250.5633	13.011	0.002	1985	Trt
58250.6223	58250.8924	12.906	0.008	199	HaC
58250.8439	58250.9865	12.783	0.003	47	SGE
58251.4100	58251.5497	2.461	0.002	669	Vih
58251.4253	58251.6246	12.925	0.003	573	BSM
58251.4465	58251.6272	13.048	0.004	295	Van
58251.6194	58251.8931	12.782	0.003	203	HaC
58251.9404	58251.9883	12.784	0.004	139	SGE
58252.4438	58252.5467	13.010	0.001	1808	Trt
58252.4535	58252.6734	13.255	0.002	499	Van
58252.4969	58252.6175	13.035	0.002	306	RJW
58252.5006	58252.6199	13.032	0.003	424	IMi
58252.6167	58252.8934	13.009	0.004	204	HaC
58252.7636	58252.8117	13.065	0.005	66	LPA
58252.8448	58252.8724	12.880	0.002	136	RIT
58252.8838	58252.9908	12.924	0.002	300	SGE
58253.4238	58253.5315	2.636	0.003	516	Vih
58253.5014	58253.6303	12.951	0.002	456	IMi
58253.5082	58253.6163	12.948	0.002	269	RJW
58253.5297	58253.6737	13.170	0.004	93	Van
58253.6116	58253.8901	12.952	0.004	205	HaC
58253.7682	58253.8648	12.939	0.002	258	LPA
58253.7874	58253.9444	13.178	0.002	370	SRI
58253.8214	58253.9792	12.943	0.002	444	SGE
58254.6088	58254.8941	12.890	0.003	211	HaC
58254.7024	58254.8166	12.833	0.002	177	LMA
58254.8120	58254.9269	12.820	0.003	138	SGE
58254.8615	58254.9349	12.859	0.002	194	LPA
58255.4888	58255.6224	12.932	0.002	344	RJW
58255.6068	58255.8933	12.993	0.011	112	HaC
58255.6322	58255.6732	13.092	0.003	94	Van
58255.8086	58255.9999	13.026	0.003	538	SGE
58256.5155	58256.6094	13.118	0.002	313	IMi
58256.5297	58256.6432	13.338	0.002	236	Van
58256.6041	58256.8920	13.094	0.005	211	HaC
58256.6868	58256.8124	13.092	0.004	208	LMA
58256.8243	58256.9117	13.041	0.002	239	SGE
58257.5002	58257.5916	13.295	0.002	204	Van
58257.5049	58257.5995	12.935	0.002	247	IMi
58257.6011	58257.8912	12.953	0.004	161	HaC
58257.6913	58257.8220	12.914	0.002	218	LMA
58257.8112	58257.9969	12.944	0.001	455	SGE
58258.4813	58258.6078	13.088	0.002	324	RJW
58258.5009	58258.5820	13.432	0.002	199	Van
58258.6013	58258.8903	13.206	0.005	172	HaC
58258.8586	58258.9966	13.197	0.003	376	SGE
58259.4066	58259.4461	13.307	0.003	119	BSM
58259.4792	58259.6168	13.221	0.003	354	RJW

Table E.1: Log of observations of the 2018 outburst in ASASSN-18ey (continued).

Start*	End*	Mag [†]	Error [‡]	N [§]	Obs
58259.5984	58259.8923	13.089	0.005	174	HaC
58259.6505	58259.6988	13.053	0.004	74	LMA
58259.6748	58259.8198	12.994	0.002	745	RIT
58260.4809	58260.6567	13.357	0.004	130	Van
58260.6704	58260.8911	13.144	0.004	119	HaC
58260.8292	58260.9710	13.033	0.002	353	SGE
58261.4276	58261.6702	13.272	0.005	177	Van
58261.4452	58261.6635	0.597	0.002	607	MLF
58261.6676	58261.8955	13.051	0.008	123	HaC
58261.8486	58261.9903	13.025	0.005	379	SGE
58262.3945	58262.5534	13.227	0.002	520	BSM
58262.4853	58262.5621	13.109	0.003	416	Trt
58262.5196	58262.5893	13.494	0.005	159	Van
58262.6647	58262.7103	13.259	0.007	27	HaC
58262.6786	58262.8636	13.194	0.002	619	RIT
58262.7914	58262.9957	13.127	0.002	570	SGE
58263.3837	58263.6165	13.198	0.002	609	BSM
58263.4054	58263.4380	13.328	0.005	55	Van
58263.6508	58263.8958	13.040	0.005	133	HaC
58263.7180	58263.8602	12.986	0.003	422	RIT
58264.3776	58264.6164	13.253	0.003	683	BSM
58264.4800	58264.5626	13.417	0.003	201	Van
58264.6481	58264.8964	13.053	0.004	134	HaC
58264.6609	58264.8380	13.030	0.003	548	RIT
58265.4175	58265.5563	13.371	0.006	119	Van
58265.5415	58265.5600	13.159	0.004	103	Trt
58265.6569	58265.8994	13.216	0.007	186	HaC
58265.7037	58265.8061	13.083	0.004	171	LMA
58266.3655	58266.6134	13.299	0.004	755	BSM
58266.6776	58266.9396	13.290	0.003	452	HaC
58266.7979	58266.9869	13.262	0.003	468	SGE
58267.6780	58267.9358	13.276	0.003	259	HaC
58267.7764	58267.9859	13.213	0.002	596	SGE
58268.6418	58268.8029	13.208	0.005	268	LMA
58268.6685	58268.9342	13.323	0.007	127	HaC
58268.7946	58268.9909	13.311	0.003	510	SGE
58269.4612	58269.5106	13.681	0.011	33	Van
58269.4848	58269.5443	13.575	0.002	329	Trt
58269.6778	58269.9341	13.478	0.007	199	HaC
58270.3581	58270.6136	13.606	0.003	802	BSM
58270.4510	58270.4927	13.771	0.004	84	Van
58270.4937	58270.5473	13.456	0.002	294	Trt
58270.7517	58270.9342	13.525	0.004	143	HaC
58270.7700	58270.8151	13.516	0.004	100	LPA
58270.8605	58270.9826	13.521	0.002	340	SGE
58271.6856	58271.9170	13.438	0.005	182	HaC
58271.8875	58271.9922	13.462	0.003	199	SGE
58271.9139	58271.9646	13.565	0.004	149	LPA
58272.2009	58272.2293	13.452	0.008	77	Kis
58272.4321	58272.6107	13.748	0.002	315	BSM
58272.4936	58272.5550	13.754	0.004	67	GCH
58272.6161	58272.6637	13.540	0.003	177	RIT

Table E.1: Log of observations of the 2018 outburst in ASASSN-18ey (continued).

Start*	End*	Mag [†]	Error [‡]	N [§]	Obs
58272.9310	58272.9835	13.340	0.004	140	SGE
58272.9782	58272.9983	13.489	0.010	32	LPA
58273.3974	58273.6108	13.514	0.004	485	BSM
58273.4839	58273.5822	13.778	0.004	244	Van
58273.8636	58273.9845	13.551	0.003	340	SGE
58274.4821	58274.5353	14.065	0.003	97	Van
58274.8055	58274.8676	13.455	0.011	39	HaC
58274.8061	58274.9915	13.452	0.003	527	SGE
58275.3940	58275.6099	13.647	0.007	491	BSM
58275.4253	58275.5078	13.401	0.009	117	EHE
58275.4889	58275.5795	13.917	0.007	222	Van
58275.5975	58275.8902	13.618	0.004	299	HaC
58275.6216	58275.8807	13.708	0.003	421	DKS
58276.3937	58276.5208	13.910	0.004	268	Van
58276.6019	58276.9229	13.699	0.008	244	HaC
58276.8000	58276.9897	13.466	0.008	540	SGE
58277.6561	58277.8503	13.614	0.006	222	RIT
58277.7265	58277.8863	13.622	0.010	102	HaC
58277.8042	58277.9908	13.523	0.004	529	SGE
58278.3331	58278.6097	13.624	0.003	614	BSM
58278.4230	58278.5057	13.910	0.004	170	Van
58278.5998	58278.8847	13.665	0.003	201	HaC
58278.6143	58278.8561	13.647	0.002	688	RIT
58278.8051	58278.9844	13.644	0.002	500	SGE
58279.4080	58279.6093	13.746	0.002	429	BSM
58279.6016	58279.8817	13.438	0.018	127	HaC
58279.8458	58279.9881	13.234	0.002	400	SGE
58279.8607	58279.9031	13.293	0.004	144	HBB
58280.3269	58280.6093	13.442	0.006	646	BSM
58280.6900	58280.8784	13.565	0.004	140	HaC
58280.8462	58280.9907	13.557	0.002	286	SGE
58281.3269	58281.6345	1.197	0.004	881	MLF
58281.4339	58281.4988	13.618	0.003	91	EHE
58281.5914	58281.8758	13.567	0.009	213	HaC
58281.8014	58281.9903	13.269	0.002	531	SGE
58281.9792	58282.0940	13.399	0.023	42	Ioh
58282.4467	58282.5720	13.573	0.008	257	BSM
58282.5638	58282.6562	13.540	0.006	72	Van
58282.5883	58282.8734	13.391	0.008	221	HaC
58282.8064	58282.9845	13.551	0.002	496	SGE
58283.3341	58283.5320	0.925	0.002	526	MLF
58283.4113	58283.6077	13.723	0.004	555	CDZ
58283.6159	58283.8484	13.579	0.002	688	RIT
58283.8119	58283.9897	13.383	0.005	510	SGE
58284.4219	58284.4564	13.918	0.008	59	Van
58284.4296	58284.6076	13.780	0.004	540	CDZ
58284.5851	58284.7994	13.240	0.005	353	LMA
58284.6111	58284.8499	13.228	0.003	568	RIT
58284.8120	58284.9903	13.332	0.004	505	SGE
58285.3748	58285.6453	13.136	0.007	490	ATE
58285.3979	58285.5796	13.506	0.007	395	Van

Table E.1: Log of observations of the 2018 outburst in ASASSN-18ey (continued).

Start*	End*	Mag [†]	Error [‡]	N [§]	Obs
58285.5803	58285.8652	13.482	0.005	213	HaC
58285.6117	58285.8497	13.479	0.002	567	RIT
58285.7729	58285.7799	13.661	0.006	10	DJE
58285.8151	58285.9554	13.468	0.003	400	SGE
58286.3816	58286.4951	13.768	0.002	220	Van
58286.4437	58286.5911	13.576	0.002	253	BSM
58286.6710	58286.7967	13.256	0.004	207	LMA
58286.7461	58286.8631	13.172	0.008	74	HaC
58286.8132	58286.9854	13.138	0.004	480	SGE
58287.3810	58287.5414	13.307	0.004	276	Van
58287.3870	58287.6587	13.085	0.003	584	ATE
58287.4120	58287.5386	13.324	0.003	370	CDZ
58287.5747	58287.8602	13.236	0.010	131	HaC
58287.8489	58287.9629	13.411	0.002	320	SGE
58287.9671	58288.0527	13.478	0.006	103	Ioh
58288.3994	58288.5797	13.708	0.002	390	Van
58288.4199	58288.5357	13.653	0.002	408	CDZ
58288.5719	58288.8569	13.358	0.011	121	HaC
58288.8481	58288.9459	12.869	0.005	285	SGE
58289.3731	58289.6434	13.292	0.009	587	ATE
58289.4125	58289.6076	13.569	0.007	623	CDZ
58289.5763	58289.8544	13.074	0.015	74	HaC
58289.5774	58289.8004	13.000	0.006	368	LMA
58289.6697	58289.6747	13.812	0.008	10	DJE
58289.8490	58289.9907	13.291	0.002	399	SGE
58290.4498	58290.5050	13.251	0.004	75	EHE
58290.5735	58290.8515	13.462	0.006	74	HaC
58290.6119	58290.8547	13.436	0.002	390	RIT
58290.6614	58290.9266	13.428	0.006	633	SJI
58290.7940	58290.9855	13.149	0.010	540	SGE
58291.3026	58291.6094	13.460	0.003	679	BSM
58291.3687	58291.5088	13.439	0.003	312	ATE
58291.3779	58291.5794	13.666	0.004	424	Van
58291.4440	58291.6329	0.846	0.005	542	MLF
58291.5716	58291.8481	13.033	0.015	64	HaC
58291.5946	58291.8081	12.912	0.007	350	LMA
58291.5966	58291.8486	12.967	0.005	778	RIT
58291.6433	58291.9266	13.074	0.006	674	SJI
58291.6987	58291.9304	13.371	0.007	532	COO
58291.8479	58291.9912	13.235	0.003	396	SGE
58292.3040	58292.6091	13.179	0.006	647	BSM
58292.4211	58292.6275	0.736	0.008	565	MLF
58292.4222	58292.5421	12.970	0.005	416	Trt
58292.4506	58292.6082	13.396	0.005	521	CDZ
58292.4979	58292.5795	13.435	0.004	183	Van
58292.5692	58292.7079	13.283	0.004	213	LMA
58292.5693	58292.8453	13.347	0.009	59	HaC
58292.6949	58292.9857	13.767	0.004	963	COO
58292.8491	58292.9835	13.170	0.006	380	SGE
58293.3037	58293.6094	13.369	0.002	673	BSM

Table E.1: Log of observations of the 2018 outburst in ASASSN-18ey (continued).

Start*	End*	Mag [†]	Error [‡]	N^{\S}	Obs
58293.3733	58293.6679	13.241	0.003	625	ATE
58293.3817	58293.6264	13.248	0.003	302	Van
58293.4165	58293.5333	13.261	0.001	608	Trt
58293.5667	58293.8427	12.952	0.020	74	HaC
58293.6426	58293.9268	12.968	0.005	672	SJI
58293.8493	58293.9841	13.068	0.005	380	SGE
58293.9673	58294.2454	13.354	0.003	613	MGW
58294.2551	58294.4214	13.245	0.009	199	OYE
58294.3795	58294.6167	12.974	0.010	164	Van
58294.5640	58294.8405	13.274	0.010	74	HaC
58294.6682	58294.7077	13.300	0.004	100	LPA
58294.6974	58294.9803	13.334	0.001	800	SGE
58294.9683	58295.2425	13.003	0.007	604	MGW
58295.3007	58295.6102	13.428	0.004	675	BSM
58295.3884	58295.5794	13.662	0.002	399	Van
58295.5597	58295.8377	13.241	0.019	103	HaC
58295.6115	58295.8531	13.126	0.008	562	RIT
58295.6357	58295.9266	13.068	0.009	694	SJI
58295.6954	58295.9460	13.267	0.006	825	COO
58295.7803	58295.9694	12.812	0.005	540	SGE
58295.9681	58296.1595	13.226	0.002	422	MGW
58296.3750	58296.6271	12.980	0.010	197	Van
58296.4706	58296.5146	12.920	0.006	62	EHE
58296.5557	58296.8336	13.129	0.013	188	HaC
58296.6761	58296.9257	13.362	0.003	592	SJI
58296.7800	58296.9697	13.328	0.002	532	SGE
58297.2513	58297.4182	13.197	0.012	200	OYE
58297.3099	58297.6105	13.311	0.004	691	BSM
58297.3652	58297.4927	13.181	0.007	61	Van
58297.4118	58297.5244	13.244	0.003	151	EHE
58297.5529	58297.8309	13.246	0.005	170	HaC
58297.6903	58297.9722	12.969	0.007	793	SGE
58298.3309	58298.4432	-0.492	0.003	367	Lic
58298.3754	58298.6263	13.082	0.013	187	Van
58298.3840	58298.6115	13.204	0.007	518	BSM
58298.4294	58298.5214	13.143	0.005	180	IMi
58298.5002	58298.5748	12.979	0.006	164	RJW
58298.5971	58298.7516	13.018	0.017	67	HaC
58298.6044	58298.8526	13.118	0.007	544	RIT
58298.6871	58298.9244	13.075	0.006	120	SGE
58299.3165	58299.6114	13.254	0.006	600	BSM
58299.3475	58299.4576	-0.759	0.004	334	Lic
58299.3663	58299.4281	13.017	0.012	32	Van
58299.4202	58299.5183	13.175	0.005	192	IMi
58299.4273	58299.5384	13.174	0.005	220	RJW
58299.4406	58299.5795	13.577	0.004	327	Van
58299.4521	58299.5345	13.220	0.004	113	EHE
58299.5493	58299.6636	13.298	0.011	49	HaC
58299.6819	58299.9675	13.246	0.011	189	SGE
58299.7942	58299.9478	12.867	0.005	504	COO

Table E.1: Log of observations of the 2018 outburst in ASASSN-18ey (continued).

Start*	End*	Mag [†]	Error [‡]	N [§]	Obs
58300.0805	58300.1387	12.952	0.007	117	Kis
58300.3395	58300.4454	-0.422	0.002	318	Lic
58300.3985	58300.5016	13.384	0.003	144	EHE
58300.4088	58300.5205	13.342	0.007	77	Van
58300.4119	58300.5156	13.375	0.003	193	IMi
58300.4274	58300.5903	13.261	0.005	354	RJW
58300.6086	58300.7397	12.909	0.005	280	RIT
58300.6790	58300.7169	12.861	0.004	109	SGE
58300.9681	58301.1891	13.389	0.001	486	MGW
58301.3312	58301.4364	-0.915	0.002	398	Lic
58301.3789	58301.5828	13.455	0.008	443	Van
58301.3924	58301.5484	13.070	0.007	429	Trt
58301.6075	58301.8473	13.301	0.002	630	RIT
58302.1146	58302.2082	13.284	0.006	208	MGW
58302.2800	58302.5325	-0.470	0.007	84	CRI
58302.2808	58302.5412	0.486	0.006	86	CRI
58302.2816	58302.5420	0.961	0.006	86	CRI
58302.2824	58302.3917	1.584	0.009	25	CRI
58302.3360	58302.4461	-0.378	0.003	278	Lic
58302.3398	58302.5444	1.025	0.002	588	MLF
58302.3648	58302.5444	13.444	0.002	462	Trt
58302.3796	58302.5831	13.814	0.002	477	Van
58302.4128	58302.6098	13.466	0.004	368	IMi
58302.4139	58302.4921	13.477	0.002	108	EHE
58302.4158	58302.5493	13.630	0.003	262	BSM
58302.4277	58302.5950	13.463	0.003	418	RJW
58302.4311	58302.6125	13.757	0.003	626	CDZ
58302.5440	58302.8184	13.173	0.017	120	HaC
58302.6827	58302.9670	13.140	0.006	800	SGE
58302.9675	58303.2085	13.471	0.001	531	MGW
58303.2727	58303.5405	0.168	0.020	54	CRI
58303.2741	58303.5350	-0.800	0.020	52	CRI
58303.2757	58303.5413	0.640	0.020	53	CRI
58303.2772	58303.5382	1.369	0.020	51	CRI
58303.3184	58303.6128	13.308	0.007	682	BSM
58303.3424	58303.5372	13.023	0.005	534	Trt
58303.3507	58303.4398	-0.778	0.006	279	Lic
58303.3718	58303.6426	13.228	0.008	675	ATE
58303.4031	58303.6288	13.208	0.014	182	Van
58303.4230	58303.5813	13.148	0.009	381	RJW
58303.4421	58303.4950	13.277	0.002	187	CDZ
58303.5411	58303.8158	13.426	0.003	127	HaC
58303.6131	58303.8504	13.410	0.002	537	RIT
58303.6845	58303.9686	13.434	0.001	800	SGE
58303.9683	58304.1383	13.170	0.006	373	MGW
58304.3113	58304.5474	0.529	0.003	52	CRI
58304.3121	58304.5482	1.013	0.004	52	CRI
58304.3150	58304.5420	-0.399	0.005	50	CRI
58304.3202	58304.5497	1.717	0.005	51	CRI
58304.3230	58304.5562	13.674	0.002	506	BSM

Table E.1: Log of observations of the 2018 outburst in ASASSN-18ey (continued).

Start*	End*	Mag [†]	Error [‡]	N [§]	Obs
58304.3407	58304.4486	-0.276	0.001	326	Lic
58304.3726	58304.6202	13.549	0.002	306	Van
58304.3844	58304.4992	13.528	0.002	153	ATE
58304.5381	58304.8126	13.327	0.017	119	HaC
58304.5982	58304.8476	13.227	0.007	504	RIT
58304.6987	58304.7329	13.175	0.006	100	SGE
58305.3188	58305.5180	-0.721	0.025	38	CRI
58305.3196	58305.5326	0.219	0.024	42	CRI
58305.3204	58305.5471	0.705	0.022	44	CRI
58305.3240	58305.5440	1.421	0.024	42	CRI
58305.3440	58305.4432	-0.557	0.006	205	Lic
58305.3816	58305.6510	13.249	0.009	181	Van
58305.4204	58305.5860	13.119	0.006	276	IMi
58305.4247	58305.4893	13.336	0.004	187	CDZ
58305.5357	58305.8108	13.355	0.008	111	HaC
58306.0931	58306.2082	13.163	0.003	255	MGW
58306.2711	58306.5425	0.416	0.007	59	CRI
58306.2719	58306.5433	0.899	0.007	59	CRI
58306.2734	58306.5448	1.630	0.007	59	CRI
58306.3007	58306.5463	-0.514	0.005	46	CRI
58306.3997	58306.6150	13.430	0.002	100	COO
58306.4170	58306.5936	13.386	0.001	447	RJW
58306.4390	58306.6147	13.698	0.002	454	CDZ
58306.4470	58306.6591	13.395	0.003	108	Van
58306.5329	58306.8081	13.357	0.009	110	HaC
58306.5415	58306.6676	13.400	0.002	312	ATE
58306.6087	58306.8544	13.231	0.005	648	RIT
58306.6950	58306.9099	13.113	0.004	561	SGE
58307.2445	58307.5858	0.938	0.004	962	MLF
58307.2831	58307.5495	0.862	0.016	59	CRI
58307.2846	58307.5510	1.595	0.017	59	CRI
58307.2861	58307.5433	-0.595	0.014	56	CRI
58307.2869	58307.5441	0.374	0.015	56	CRI
58307.3571	58307.4417	-0.406	0.003	332	Lic
58307.3741	58307.5165	1.422	0.031	15	Lis
58307.3742	58307.5164	0.854	0.002	1897	Lis
58307.3743	58307.5166	0.250	0.028	15	Lis
58307.3745	58307.5167	-0.765	0.022	15	Lis
58307.3747	58307.5068	-2.370	0.028	14	Lis
58307.3769	58307.6594	13.199	0.005	236	Van
58307.4168	58307.5947	13.200	0.003	452	RJW
58307.4336	58307.6088	13.502	0.003	423	CDZ
58307.4936	58307.6495	13.169	0.003	318	ATE
58307.5302	58307.8036	13.251	0.008	114	HaC
58307.5898	58307.8331	13.252	0.003	483	RIT
58307.5919	58307.8572	13.566	0.004	397	SDB
58307.6912	58307.9357	13.673	0.001	602	COO
58307.7458	58307.7497	13.274	0.003	12	SGE
58308.2511	58308.4182	13.195	0.004	200	OYE
58308.2707	58308.5752	0.827	0.002	844	MLF

Table E.1: Log of observations of the 2018 outburst in ASASSN-18ey (continued).

Start*	End*	Mag [†]	Error [‡]	N [§]	Obs
58308.2883	58308.3388	-0.763	0.009	12	CRI
58308.2891	58308.3450	0.353	0.076	16	CRI
58308.2898	58308.3312	0.676	0.013	10	CRI
58308.2913	58308.3373	1.380	0.011	11	CRI
58308.3347	58308.4468	-0.568	0.001	279	Lic
58308.3672	58308.6206	13.246	0.001	375	Van
58308.4161	58308.5953	13.257	0.001	458	RJW
58308.5296	58308.7966	13.249	0.002	111	HaC
58308.5928	58308.8703	13.502	0.002	415	SDB
58308.6041	58308.8510	13.191	0.001	530	RIT
58308.7589	58308.9375	13.044	0.008	163	SGE
58309.0532	58309.2910	0.862	0.002	658	KU1
58309.0932	58309.2042	13.272	0.002	243	MGW
58309.2771	58309.5299	-0.664	0.008	56	CRI
58309.2787	58309.5406	0.725	0.010	58	CRI
58309.2802	58309.5513	1.443	0.010	60	CRI
58309.2825	58309.5398	0.267	0.009	57	CRI
58309.3410	58309.4461	-0.519	0.001	255	Lic
58309.3602	58309.6622	13.161	0.004	740	ATE
58309.3650	58309.6660	13.143	0.006	318	Van
58309.4324	58309.6173	13.435	0.003	536	CDZ
58309.5252	58309.7985	13.099	0.005	116	HaC
58309.5912	58309.8322	13.095	0.003	532	RIT
58309.6936	58309.9169	13.126	0.002	599	SGE
58309.7970	58309.8888	12.874	0.001	219	COO
58309.9784	58310.0695	-0.502	0.002	108	KU2
58310.0101	58310.2018	13.149	0.002	399	MGW
58310.0709	58310.2925	0.652	0.001	1696	KU1
58310.3271	58310.5830	13.272	0.003	578	BSM
58310.3442	58310.4453	-0.767	0.005	73	Lic
58310.3446	58310.4156	-0.580	0.006	53	Lic
58310.3450	58310.4448	-0.348	0.005	74	Lic
58310.3666	58310.6429	13.166	0.003	327	Van
58310.4146	58310.5967	13.164	0.001	454	RJW
58310.4869	58310.6180	13.531	0.003	100	CDZ
58310.5783	58310.8044	13.151	0.001	221	LMA
58310.6420	58310.8574	13.539	0.003	346	SJP
58310.6804	58310.9170	13.488	0.004	602	SGE
58310.7115	58310.7953	13.178	0.005	35	HaC
58311.0097	58311.1991	13.011	0.003	416	MGW
58311.3220	58311.5808	13.304	0.003	589	BSM
58311.3449	58311.4413	-0.631	0.005	55	Lic
58311.3454	58311.4418	-0.422	0.005	55	Lic
58311.3460	58311.4424	-0.205	0.004	55	Lic
58311.3655	58311.6654	13.109	0.010	182	Van
58311.3820	58311.6657	13.082	0.003	699	ATE
58311.4362	58311.6189	13.387	0.002	610	CDZ
58311.5066	58311.5477	13.111	0.002	68	IMi
58311.5948	58311.8515	12.937	0.003	649	RIT
58311.6169	58311.8473	13.340	0.003	502	CDJ

Table E.1: Log of observations of the 2018 outburst in ASASSN-18ey (continued).

Start*	End*	Mag [†]	Error [‡]	N [§]	Obs
58311.8357	58311.8742	12.999	0.002	108	SGE
58311.9275	58312.1961	13.125	0.002	533	MGW
58312.0588	58312.2624	13.333	0.007	66	Ioh
58312.0601	58312.2712	13.162	0.006	70	Ioh
58312.3204	58312.5829	13.062	0.004	591	BSM
58312.3267	58312.4381	-1.005	0.005	69	Lic
58312.3272	58312.4385	-0.807	0.005	69	Lic
58312.3278	58312.4366	-0.577	0.004	70	Lic
58312.3535	58312.5310	12.878	0.003	449	Trt
58312.3652	58312.5799	13.087	0.005	252	GCH
58312.3770	58312.6569	12.948	0.011	137	Van
58312.4179	58312.5244	12.941	0.002	247	RJW
58312.4272	58312.6039	13.308	0.003	535	CDZ
58312.4324	58312.5380	2.417	0.004	207	Vih
58312.4722	58312.6175	13.020	0.003	275	IMi
58312.5708	58312.7808	13.018	0.002	252	LMA
58312.9257	58313.1935	12.910	0.003	504	MGW
58312.9818	58313.2683	0.483	0.003	2053	KU1
58313.0070	58313.2503	13.046	0.010	102	Ioh
58313.0084	58313.2510	12.903	0.009	114	Ioh
58313.3208	58313.5829	13.140	0.002	598	BSM
58313.3599	58313.6410	12.991	0.002	673	ATE
58313.3783	58313.6662	13.003	0.003	182	Van
58313.4056	58313.5082	13.000	0.003	224	Trt
58313.4132	58313.5957	13.018	0.002	466	RJW
58313.4272	58313.6195	13.321	0.001	671	CDZ
58313.4292	58313.4995	13.180	0.004	76	GCH
58313.4687	58313.6074	12.999	0.002	269	IMi
58313.5144	58313.7112	12.963	0.005	86	HaC
58313.7192	58313.9243	12.875	0.005	470	SGE
58313.9258	58314.1909	13.119	0.002	586	MGW
58313.9661	58314.2757	0.650	0.001	2359	KU1
58313.9925	58314.1788	13.187	0.003	191	Nel
58314.0401	58314.1884	13.161	0.008	43	Ioh
58314.0408	58314.1821	13.337	0.011	35	Ioh
58314.3435	58314.4338	-1.042	0.014	34	Lic
58314.3441	58314.4343	-0.779	0.010	63	Lic
58314.3447	58314.4350	-0.607	0.015	33	Lic
58314.3589	58314.5828	12.915	0.004	526	BSM
58314.3633	58314.4473	12.774	0.009	114	Van
58314.3908	58314.5131	12.707	0.003	259	Trt
58314.4085	58314.6174	13.100	0.004	730	CDZ
58314.4226	58314.5940	12.783	0.004	427	RJW
58314.4837	58314.6127	12.854	0.006	228	IMi
58314.5172	58314.7846	12.946	0.007	103	HaC
58314.6827	58314.9152	13.011	0.003	474	SGE
58314.9254	58315.1881	12.879	0.006	581	MGW
58314.9820	58315.0991	12.975	0.010	117	Nel
58314.9908	58315.2929	0.485	0.003	2183	KU1
58315.1351	58315.2611	13.070	0.017	80	Ioh

Table E.1: Log of observations of the 2018 outburst in ASASSN-18ey (continued).

Start*	End*	Mag [†]	Error [‡]	N [§]	Obs
58315.1365	58315.2740	12.881	0.012	97	Ioh
58315.2497	58315.4167	13.044	0.002	200	OYE
58315.3208	58315.4305	-0.811	0.004	58	Lic
58315.3213	58315.4310	-0.607	0.004	58	Lic
58315.3220	58315.4317	-0.392	0.004	58	Lic
58315.3405	58315.5083	13.040	0.002	464	Trt
58315.3679	58315.4733	13.219	0.002	113	GCH
58315.3760	58315.4476	13.059	0.002	93	Van
58315.4084	58315.5728	13.101	0.001	415	RJW
58315.5094	58315.7833	13.004	0.011	104	HaC
58315.5694	58315.7612	12.939	0.005	228	LMA
58315.6134	58315.8427	12.875	0.005	484	RIT
58315.6821	58315.9402	12.804	0.004	698	SGE
58315.9256	58316.1853	13.073	0.002	574	MGW
58316.0930	58316.2585	0.789	0.002	1264	KU1
58316.3225	58316.5830	13.147	0.002	524	BSM
58316.3578	58316.6653	13.034	0.002	724	ATE
58316.3641	58316.6660	13.055	0.004	229	Van
58316.4070	58316.6119	13.298	0.002	722	CDZ
58316.4432	58316.4832	12.989	0.003	37	EHE
58316.4605	58316.6140	12.998	0.004	297	IMi
58316.5064	58316.7806	13.066	0.005	116	HaC
58316.5308	58316.5431	1.044	0.011	10	Lis
58316.5310	58316.5433	0.514	0.009	10	Lis
58316.5312	58316.5436	-0.076	0.010	10	Lis
58316.6408	58316.8340	13.463	0.001	420	CDJ
58316.6743	58316.9200	13.105	0.001	680	SGE
58316.9259	58317.1827	13.084	0.004	532	MGW
58317.0053	58317.1831	12.963	0.006	69	Ioh
58317.0156	58317.1757	13.074	0.010	49	Ioh
58317.0947	58317.2609	0.630	0.001	1076	KU1
58317.2580	58317.5334	0.671	0.003	756	MLF
58317.3786	58317.6549	13.168	0.004	192	Van
58317.4059	58317.6090	13.440	0.002	709	CDZ
58317.5806	58317.7783	13.110	0.010	83	HaC
58317.6230	58317.8207	13.034	0.004	450	RIT
58317.6742	58317.9172	12.927	0.004	573	SGE
58317.9254	58318.1700	13.141	0.003	539	MGW
58318.0134	58318.2621	0.779	0.001	1831	KU1
58318.0156	58318.2032	13.238	0.002	213	Nel
58318.2498	58318.4168	13.169	0.002	200	OYE
58318.3253	58318.5689	13.154	0.004	475	BSM
58318.3292	58318.4252	0.714	0.002	209	MLF
58318.3608	58318.6694	12.928	0.004	379	Van
58318.3652	58318.6507	12.964	0.004	711	ATE
58318.4050	58318.6063	13.251	0.003	704	CDZ
58318.4247	58318.5076	13.048	0.005	85	EHE
58318.5612	58318.7422	12.903	0.006	218	LMA
58318.6007	58318.8290	13.005	0.005	521	RIT
58318.6648	58318.8297	13.437	0.003	359	CDJ

Table E.1: Log of observations of the 2018 outburst in ASASSN-18ey (continued).

Start*	End*	Mag [†]	Error [‡]	N [§]	Obs
58318.9048	58319.1232	13.165	0.001	482	MGW
58318.9761	58319.1880	0.726	0.001	1569	KU1
58319.3010	58319.3925	0.616	0.003	204	MLF
58319.3244	58319.5831	13.238	0.003	582	BSM
58319.3695	58319.6290	13.138	0.003	293	Van
58319.4039	58319.6034	13.428	0.002	616	CDZ
58319.6731	58319.9020	13.024	0.003	552	SGE
58319.7170	58319.9145	13.083	0.003	433	JJI
58319.9049	58320.1474	13.016	0.004	457	MGW
58319.9541	58320.1919	0.638	0.003	917	KU1
58320.1891	58320.2792	13.264	0.011	62	Ioh
58320.1898	58320.2620	13.353	0.013	42	Ioh
58320.3899	58320.6472	13.096	0.004	259	Van
58320.4061	58320.4485	13.487	0.001	113	CDZ
58320.4093	58320.5233	3.057	0.001	266	Vih
58320.5724	58320.6804	13.029	0.004	45	HaC
58320.6785	58320.8998	13.129	0.002	597	SGE
58320.7375	58320.7800	13.280	0.004	65	DJE
58320.9046	58321.0871	13.254	0.001	402	MGW
58321.1174	58321.2044	13.243	0.005	53	Ioh
58321.1180	58321.2037	13.400	0.009	45	Ioh
58321.1595	58321.2506	0.754	0.001	707	KU1
58321.2486	58321.4161	13.296	0.003	199	OYE
58321.3242	58321.5725	13.319	0.005	438	BSM
58321.3630	58321.6558	13.252	0.006	293	Van
58321.3841	58321.4820	3.119	0.003	165	Vih
58321.5648	58321.7406	13.284	0.002	210	LMA
58321.6776	58321.8969	13.204	0.003	543	SGE
58321.7298	58321.9425	13.245	0.003	475	JJI
58321.9048	58322.1687	13.106	0.003	583	MGW
58322.0330	58322.0696	13.230	0.009	28	Ioh
58322.0343	58322.1072	13.092	0.012	30	Ioh
58322.0496	58322.1433	13.189	0.006	103	Nel
58322.1537	58322.2771	0.915	0.002	955	KU1
58322.3523	58322.6430	13.244	0.003	688	ATE
58322.3611	58322.6428	13.207	0.007	166	Van
58322.4015	58322.5952	13.544	0.003	677	CDZ
58322.4457	58322.5281	13.352	0.002	88	EHE
58322.5669	58322.7627	13.024	0.008	83	HaC
58322.6817	58322.9018	13.054	0.004	599	SGE
58322.7090	58322.9399	13.206	0.004	535	JJI
58322.9051	58323.0051	13.282	0.002	221	MGW
58322.9625	58323.2631	13.288	0.005	207	Ioh
58322.9632	58323.2499	13.442	0.005	201	Ioh
58323.1265	58323.2364	0.767	0.002	854	KU1
58323.2882	58323.4765	-0.794	0.010	38	CRI
58323.2891	58323.4773	0.108	0.010	37	CRI
58323.2898	58323.4781	0.568	0.010	37	CRI
58323.2913	58323.4750	1.291	0.009	38	CRI
58323.3524	58323.6456	13.179	0.009	153	Van

Table E.1: Log of observations of the 2018 outburst in ASASSN-18ey (continued).

Start*	End*	Mag [†]	Error [‡]	N [§]	Obs
58323.4076	58323.5085	13.166	0.008	89	EHE
58323.4248	58323.5925	13.524	0.003	577	CDZ
58323.6709	58323.9001	13.201	0.002	643	SGE
58323.7016	58323.9370	13.300	0.002	550	JJI
58323.8838	58324.1634	13.106	0.003	617	MGW
58324.1292	58324.2413	0.770	0.003	869	KU1
58324.3993	58324.5895	13.623	0.001	664	CDZ
58324.4130	58324.4965	13.348	0.002	78	EHE
58324.5641	58324.7472	13.138	0.013	83	HaC
58324.6435	58324.8131	13.401	0.002	385	CDJ
58324.7055	58324.9346	13.187	0.004	504	JJI
58324.8840	58325.1609	13.302	0.002	611	MGW
58325.2980	58325.5503	-0.751	0.011	52	CRI
58325.2988	58325.5487	0.132	0.007	50	CRI
58325.2996	58325.5495	0.589	0.008	51	CRI
58325.3011	58325.5454	1.303	0.009	50	CRI
58325.3312	58325.5552	13.224	0.002	506	BSM
58325.3983	58325.5011	13.056	0.002	243	RJW
58325.3995	58325.5869	13.448	0.005	402	CDZ
58325.6235	58325.7605	13.612	0.002	297	CDJ
58325.7100	58325.9316	13.346	0.001	481	JJI
58325.9123	58326.0639	13.243	0.003	273	MGW
58326.3738	58326.5553	13.448	0.002	377	BSM
58326.3973	58326.4792	13.615	0.002	283	CDZ
58326.4049	58326.5000	13.301	0.004	65	Van
58326.6226	58326.8024	13.527	0.001	332	CDJ
58326.7287	58326.9289	13.228	0.002	449	JJI
58327.3439	58327.5053	3.009	0.003	377	Vih
58327.3855	58327.5550	13.272	0.003	354	BSM
58327.3998	58327.4992	13.135	0.007	63	Van
58327.4043	58327.5814	13.473	0.003	349	CDZ
58327.4480	58327.5099	13.127	0.004	80	EHE
58327.5557	58327.7507	13.242	0.005	92	HaC
58327.7003	58327.9264	13.353	0.001	470	JJI
58328.3271	58328.5030	2.968	0.001	403	Vih
58328.3655	58328.4999	13.499	0.002	208	Van
58328.5537	58328.7483	13.205	0.005	84	HaC
58328.7250	58328.9236	13.169	0.002	465	JJI
58328.9965	58329.2333	13.395	0.005	163	Ioh
58328.9972	58329.2492	13.251	0.005	183	Ioh
58329.2529	58329.4196	13.441	0.001	199	OYE
58329.3206	58329.5412	13.283	0.002	475	BSM
58329.3409	58329.4290	2.995	0.001	180	Vih
58329.3442	58329.5162	13.295	0.002	199	GCH
58329.3772	58329.6076	13.117	0.003	125	Van
58329.4049	58329.5109	13.449	0.001	237	CDZ
58329.6676	58329.9290	13.240	0.002	291	SRI
58329.8626	58330.1459	13.236	0.001	841	MGW
58329.9684	58330.0725	13.258	0.003	84	Nel
58330.3184	58330.5271	13.321	0.002	453	BSM

Table E.1: Log of observations of the 2018 outburst in ASASSN-18ey (continued).

Start*	End*	Mag [†]	Error [‡]	N [§]	Obs
58330.3503	58330.5614	13.212	0.001	516	ATE
58330.3933	58330.4937	13.491	0.001	348	CDZ
58330.4111	58330.5073	13.529	0.001	155	Van
58330.5481	58330.7424	13.243	0.003	92	HaC
58330.6106	58330.7191	13.201	0.001	130	LMA
58330.6858	58330.9110	13.588	0.001	608	COO
58330.8628	58331.1443	13.207	0.001	836	MGW
58331.3163	58331.5269	13.431	0.002	223	BSM
58331.3881	58331.4759	13.211	0.002	223	RJW
58331.3896	58331.5552	13.558	0.001	284	Van
58331.3926	58331.5700	13.499	0.001	619	CDZ
58331.6047	58331.7193	13.117	0.001	136	LMA
58331.8630	58332.1414	13.274	0.001	830	MGW
58332.2425	58332.4834	0.728	0.002	444	MLF
58332.3103	58332.5269	13.340	0.004	249	BSM
58332.3277	58332.5097	13.339	0.003	208	GCH
58332.3584	58332.5551	13.572	0.002	328	Van
58332.3911	58332.5674	13.519	0.001	614	CDZ
58332.6672	58332.8480	13.219	0.001	500	SGE
58332.7364	58332.7938	13.624	0.001	133	CDJ
58332.8628	58333.1038	13.223	0.001	673	MGW
58333.0564	58333.2253	13.286	0.006	96	Ioh
58333.0570	58333.2054	13.483	0.008	106	Ioh
58333.2364	58333.4134	0.855	0.001	486	MLF
58333.3267	58333.5180	3.121	0.001	375	Vih
58333.3396	58333.5267	13.443	0.002	194	BSM
58333.3490	58333.4772	13.315	0.003	84	ATE
58333.3606	58333.5548	13.657	0.002	312	Van
58333.3819	58333.5411	13.260	0.001	392	RJW
58333.3887	58333.5646	13.577	0.001	602	CDZ
58333.3935	58333.5100	13.293	0.003	107	EHE
58333.5831	58333.6833	13.174	0.002	121	LMA
58333.6639	58333.8449	13.250	0.003	491	SGE
58334.2022	58334.4478	0.811	0.002	706	MLF
58334.3139	58334.4567	13.179	0.001	404	Trt
58334.3574	58334.5140	13.605	0.003	258	Van
58334.3635	58334.4736	3.048	0.002	217	Vih
58334.3805	58334.5392	13.210	0.002	405	RJW
58334.3893	58334.3993	13.207	0.003	26	CDZ
58334.3999	58334.5147	13.237	0.003	131	EHE
58334.5807	58334.8513	13.607	0.002	616	SJP
58335.0335	58335.2058	13.218	0.007	177	Ioh
58335.2435	58335.4104	13.251	0.001	200	OYE
58335.3140	58335.4547	13.210	0.001	398	Trt
58335.3687	58335.4816	13.257	0.002	160	Van
58335.3733	58335.4731	13.224	0.001	135	PXR
58335.3871	58335.5590	13.260	0.001	374	CDZ
58335.5561	58335.7591	13.357	0.002	416	DKS
58335.8728	58335.9285	13.363	0.004	65	Nel
58336.0655	58336.2071	13.395	0.004	176	Ioh

Table E.1: Log of observations of the 2018 outburst in ASASSN-18ey (continued).

Start*	End*	Mag [†]	Error [‡]	N [§]	Obs
58336.2419	58336.4445	0.476	0.002	581	MLF
58336.3569	58336.4992	13.568	0.001	234	Van
58336.3762	58336.4530	13.202	0.002	218	Trt
58336.3773	58336.5332	13.224	0.001	392	RJW
58336.3873	58336.4033	13.266	0.002	41	CDZ
58336.3999	58336.5037	13.239	0.001	134	EHE
58336.5441	58336.7260	13.307	0.002	85	HaC
58336.5525	58336.7190	13.425	0.002	203	MZK
58336.5661	58336.7205	13.300	0.001	330	DKS
58336.5729	58336.7521	13.272	0.001	205	SDB
58336.5896	58336.7521	13.297	0.002	169	RIT
58336.6609	58336.8802	13.344	0.001	248	SRI
58336.6949	58336.9016	13.446	0.002	439	JJI
58337.3112	58337.4077	3.203	0.001	162	Vih
58337.3557	58337.4704	13.635	0.002	184	Van
58337.3614	58337.4499	13.260	0.001	251	Trt
58337.3835	58337.5014	13.312	0.002	143	EHE
58337.3939	58337.5303	13.295	0.001	345	RJW
58337.5132	58337.5541	13.362	0.003	80	CDZ
58337.5493	58337.7070	13.325	0.001	329	DKS
58337.5541	58337.7226	13.337	0.003	79	HaC
58337.6620	58337.8365	13.295	0.004	214	SRI
58337.8847	58338.1040	13.321	0.001	651	MGW
58338.2979	58338.4979	3.116	0.002	467	Vih
58338.3966	58338.5011	13.229	0.003	132	EHE
58338.4004	58338.5513	13.216	0.002	375	CDZ
58338.5266	58338.7179	13.237	0.005	90	HaC
58338.5498	58338.7568	13.247	0.002	423	DKS
58338.5585	58338.7551	13.231	0.002	235	LMA
58338.6589	58338.8778	13.322	0.002	250	SRI
58339.2993	58339.4299	13.307	0.002	95	BSM
58339.3108	58339.4661	3.155	0.001	353	Vih
58339.3168	58339.4454	13.258	0.002	364	Trt
58339.3642	58339.5002	13.622	0.002	231	Van
58339.3842	58339.4631	13.313	0.001	171	CDZ
58339.5247	58339.7173	13.384	0.004	78	HaC
58339.5772	58339.7717	13.559	0.001	417	BMS
58339.6998	58339.8312	13.364	0.002	160	SRI
58339.9065	58340.1198	13.300	0.001	633	MGW
58340.0747	58340.1867	13.377	0.006	52	Ioh
58340.0754	58340.1860	13.591	0.011	48	Ioh
58340.3020	58340.4044	13.409	0.003	72	BSM
58340.3251	58340.4917	3.302	0.002	389	Vih
58340.3848	58340.5459	13.371	0.003	192	CDZ
58340.4050	58340.5414	13.370	0.004	131	Van
58340.5249	58340.7126	13.293	0.003	77	HaC
58340.5421	58340.7126	13.407	0.002	209	MZK
58340.6592	58340.8616	13.349	0.002	396	SGE
58340.9821	58341.1032	13.428	0.006	47	Ioh
58340.9828	58341.1039	13.595	0.007	43	Ioh

Table E.1: Log of observations of the 2018 outburst in ASASSN-18ey (continued).

Start*	End*	Mag [†]	Error [‡]	N^{\S}	Obs
58341.3006	58341.5024	13.419	0.002	167	BSM
58341.3570	58341.4806	3.314	0.001	253	Vih
58341.3934	58341.5305	13.375	0.001	124	Van
58341.5212	58341.7103	13.429	0.003	80	HaC
58341.5785	58341.7499	13.434	0.001	316	DKS
58341.6579	58341.7842	13.449	0.002	201	SGE
58342.2555	58342.4217	13.487	0.001	200	OYE
58342.3545	58342.5026	13.470	0.003	129	BSM
58342.3574	58342.4339	13.782	0.002	130	Van
58342.3666	58342.4549	13.467	0.002	112	EHE
58342.5136	58342.7072	13.292	0.004	82	HaC
58342.6006	58342.7466	13.278	0.001	279	DKS
58342.6566	58342.7401	13.285	0.002	121	SGE
58342.7338	58342.7540	13.275	0.017	26	DJE
58342.9815	58343.1382	1.398	0.003	37	KU2
58342.9822	58343.1419	0.983	0.003	38	KU2
58342.9829	58343.1426	0.549	0.004	35	KU2
58342.9836	58343.1252	-0.196	0.003	26	KU2
58343.3389	58343.4874	3.154	0.002	346	Vih
58343.3937	58343.5305	13.295	0.001	217	Van
58343.4128	58343.5657	13.327	0.004	75	DFS
58343.5129	58343.7051	13.386	0.004	81	HaC
58343.5792	58343.7566	13.608	0.001	396	NOM
58343.6589	58343.7906	13.406	0.001	200	SGE
58343.9052	58344.1041	13.311	0.001	459	MGW
58344.0645	58344.2057	1.307	0.003	43	KU2
58344.0652	58344.2094	0.906	0.003	42	KU2
58344.0659	58344.2072	0.484	0.006	35	KU2
58344.0667	58344.1289	-0.248	0.007	20	KU2
58344.3136	58344.4661	3.320	0.002	353	Vih
58344.3669	58344.5155	13.436	0.002	107	COO
58344.3929	58344.5310	13.404	0.002	88	Van
58344.3979	58344.4167	13.383	0.003	25	PXR
58344.5100	58344.7018	13.371	0.005	78	HaC
58344.6595	58344.8467	13.300	0.002	300	SGE
58344.8783	58345.0215	13.313	0.004	149	Nel
58344.9055	58345.1042	13.393	0.001	591	MGW
58344.9756	58345.1350	1.380	0.003	53	KU2
58344.9764	58345.1357	0.967	0.003	48	KU2
58344.9771	58345.1155	0.543	0.003	45	KU2
58344.9828	58345.1808	13.628	0.005	102	Ioh
58344.9835	58345.2064	13.417	0.004	101	Ioh
58345.0075	58345.1133	-0.179	0.005	24	KU2
58345.2945	58345.3925	13.306	0.004	61	BSM
58345.3377	58345.5119	13.260	0.001	431	ATE
58345.3615	58345.4595	13.226	0.001	247	RJW
58345.3859	58345.5211	13.302	0.002	87	Van
58345.5199	58345.7012	13.328	0.004	75	HaC
58345.6520	58345.8294	13.386	0.001	200	SRI
58345.6571	58345.8445	13.362	0.001	300	SGE

Table E.1: Log of observations of the 2018 outburst in ASASSN-18ey (continued).

Start*	End*	Mag [†]	Error [‡]	N [§]	Obs
58346.3459	58346.5001	13.779	0.003	270	Van
58346.3459	58346.5001	13.783	0.003	270	Van
58346.4090	58346.4872	13.495	0.003	103	EHE
58346.5170	58346.6985	13.435	0.005	74	HaC
58346.6022	58346.6963	13.525	0.004	115	MZK
58346.6530	58346.8403	13.302	0.002	300	SGE
58346.9407	58347.0485	13.461	0.004	122	Nel
58347.2954	58347.4845	13.302	0.007	112	BSM
58347.3397	58347.4562	3.181	0.004	221	Vih
58347.3418	58347.4302	13.638	0.004	148	Van
58347.3418	58347.4302	13.643	0.004	148	Van
58347.3514	58347.4653	13.274	0.004	151	EHE
58347.5157	58347.6957	13.335	0.003	74	HaC
58347.5297	58347.6707	13.309	0.002	144	LMA
58347.6519	58347.8390	13.387	0.003	300	SGE
58347.9427	58348.2094	1.377	0.005	85	KU2
58347.9435	58348.2042	0.949	0.004	83	KU2
58347.9442	58348.1990	0.513	0.004	77	KU2
58347.9449	58348.1612	-0.215	0.004	68	KU2
58348.0047	58348.1844	13.541	0.004	95	Ioh
58348.0054	58348.1892	13.372	0.005	100	Ioh
58348.2782	58348.4144	-0.595	0.004	30	CRI
58348.2790	58348.4152	0.340	0.004	30	CRI
58348.2820	58348.4175	1.521	0.005	30	CRI
58348.2970	58348.4843	13.368	0.003	93	BSM
58348.2977	58348.4673	3.223	0.001	331	Vih
58348.3356	58348.5063	13.330	0.001	416	ATE
58348.3392	58348.5101	13.691	0.002	273	Van
58348.3752	58348.4723	13.344	0.002	136	EHE
58348.5116	58348.6928	13.316	0.003	74	HaC
58348.9503	58349.1279	1.296	0.004	39	KU2
58348.9511	58349.1227	0.879	0.004	35	KU2
58348.9518	58349.1264	0.457	0.005	34	KU2
58348.9585	58349.1271	-0.258	0.008	29	KU2
58349.2887	58349.4537	3.276	0.001	322	Vih
58349.3422	58349.5099	13.736	0.002	262	Van
58349.4027	58349.4766	13.375	0.003	99	EHE
58349.5256	58349.6901	13.314	0.003	75	HaC
58349.5437	58349.6261	13.315	0.001	129	DKS
58349.6502	58349.7723	13.383	0.001	192	SGE
58349.6833	58349.7798	13.418	0.002	111	EEY
58349.9283	58350.1736	1.432	0.003	76	KU2
58349.9291	58350.1743	1.007	0.004	75	KU2
58349.9298	58350.1662	0.577	0.004	73	KU2
58349.9335	58350.1120	-0.149	0.004	53	KU2
58350.2382	58350.4249	-0.605	0.010	41	CRI
58350.2390	58350.4211	0.322	0.008	40	CRI
58350.2398	58350.4265	0.785	0.007	41	CRI
58350.2420	58350.4280	1.536	0.010	41	CRI
58350.2590	58350.4178	13.557	0.003	187	OYE

Table E.1: Log of observations of the 2018 outburst in ASASSN-18ey (continued).

Start*	End*	Mag [†]	Error [‡]	N^{\S}	Obs
58350.3040	58350.4417	3.157	0.001	269	Vih
58350.5228	58350.6880	13.391	0.003	75	HaC
58350.6696	58350.7930	13.399	0.001	200	SGE
58350.8859	58351.0870	13.300	0.003	385	MGW
58351.2864	58351.4594	3.293	0.002	404	Vih
58351.2885	58351.4158	-0.491	0.008	28	CRI
58351.2893	58351.4166	0.430	0.006	28	CRI
58351.2901	58351.4174	0.911	0.007	28	CRI
58351.2937	58351.4189	1.639	0.009	28	CRI
58351.4742	58351.5422	13.392	0.002	110	Van
58351.5183	58351.6832	13.332	0.003	110	HaC
58351.6116	58351.8060	13.417	0.002	465	SJI
58351.6481	58351.8345	13.418	0.002	300	SGE
58351.9466	58352.1467	1.469	0.003	58	KU2
58351.9473	58352.1445	1.052	0.003	59	KU2
58351.9480	58352.1452	0.619	0.003	55	KU2
58351.9487	58352.1459	-0.121	0.003	43	KU2
58352.2688	58352.3581	-0.683	0.021	20	CRI
58352.2740	58352.4071	1.607	0.006	30	CRI
58352.2763	58352.4048	0.440	0.015	26	CRI
58352.2817	58352.4056	0.936	0.011	26	CRI
58352.3114	58352.3690	3.254	0.002	135	Vih
58352.3517	58352.4591	13.447	0.003	272	RJW
58352.3864	58352.4687	13.495	0.002	114	EHE
58352.5007	58352.6818	13.478	0.003	124	HaC
58352.6472	58352.8408	13.524	0.002	287	SGE
58352.8861	58353.0844	13.424	0.001	588	MGW
58352.9419	58353.1514	1.434	0.003	61	KU2
58352.9426	58353.1699	1.026	0.003	72	KU2
58352.9433	58353.1757	0.596	0.003	73	KU2
58352.9441	58353.1535	-0.142	0.005	51	KU2
58353.2737	58353.4494	3.308	0.001	410	Vih
58353.2828	58353.4136	-0.419	0.006	27	CRI
58353.2836	58353.4144	0.509	0.004	28	CRI
58353.2844	58353.4152	0.959	0.005	28	CRI
58353.2880	58353.4167	1.680	0.010	28	CRI
58353.3856	58353.4591	13.473	0.004	86	EHE
58353.5499	58353.7508	13.393	0.002	163	SDB
58353.6461	58353.8395	13.469	0.002	300	SGE
58353.8639	58354.0625	13.547	0.001	590	MGW
58354.2871	58354.3416	3.304	0.001	122	Vih
58354.3260	58354.4620	13.498	0.002	214	ATE
58354.3636	58354.5069	13.509	0.002	345	CDZ
58354.5100	58354.6764	13.487	0.003	112	HaC
58354.5517	58354.7454	13.519	0.003	156	SDB
58354.5987	58354.7046	13.477	0.007	85	RIT
58354.8748	58355.0444	13.485	0.005	174	Nel
58355.0393	58355.1796	13.498	0.007	86	Ioh
58355.0428	58355.1693	13.721	0.008	75	Ioh
58355.3504	58355.4785	13.532	0.002	198	Van

Table E.1: Log of observations of the 2018 outburst in ASASSN-18ey (continued).

Start*	End*	Mag [†]	Error [‡]	N^{\S}	Obs
58355.5087	58355.6734	13.456	0.008	75	HaC
58355.6443	58355.7679	13.361	0.002	191	SGE
58355.9467	58356.1758	1.494	0.003	68	KU2
58355.9474	58356.1765	1.090	0.004	65	KU2
58355.9481	58356.1743	0.669	0.004	65	KU2
58355.9488	58356.1483	-0.048	0.005	51	KU2
58355.9697	58356.1699	13.574	0.004	142	Ioh
58355.9704	58356.1664	13.742	0.006	139	Ioh
58356.3501	58356.4983	13.318	0.004	114	Van
58356.3506	58356.4876	13.378	0.006	90	BSM
58356.4212	58356.5014	13.410	0.005	200	CDZ
58356.5062	58356.6708	13.417	0.003	82	HaC
58356.6432	58356.7660	13.495	0.002	200	SGE
58356.9333	58357.1731	1.388	0.009	71	KU2
58356.9340	58357.1827	0.968	0.007	76	KU2
58356.9348	58357.1834	0.552	0.007	67	KU2
58356.9352	58357.1545	13.435	0.005	159	Ioh
58356.9355	58357.1338	-0.161	0.008	52	KU2
58356.9359	58357.1276	13.609	0.006	137	Ioh
58357.2994	58357.4545	13.469	0.004	104	BSM
58357.3502	58357.4983	13.450	0.002	119	Van
58357.5032	58357.6554	13.506	0.004	99	HaC
58357.5750	58357.6557	13.541	0.008	67	RIT
58357.5750	58357.6557	13.557	0.008	67	RIT
58357.6423	58357.7654	13.545	0.003	200	SGE
58357.8726	58358.0624	13.500	0.001	566	MGW
58358.0006	58358.1619	1.514	0.004	30	KU2
58358.0013	58358.1655	1.130	0.006	30	KU2
58358.0020	58358.1633	0.712	0.006	26	KU2
58358.2744	58358.4298	3.344	0.002	346	Vih
58358.3502	58358.4871	13.470	0.003	103	Van
58358.3579	58358.4964	13.526	0.002	262	CDZ
58358.3597	58358.5245	13.473	0.001	392	ATE
58358.4918	58358.6656	13.479	0.002	111	HaC
58358.6411	58358.7724	13.526	0.002	204	SGE
58359.2922	58359.3446	3.355	0.002	116	Vih
58359.2946	58359.4506	13.598	0.003	105	BSM
58359.3243	58359.4904	13.534	0.001	378	ATE
58359.3474	58359.4805	13.546	0.001	201	Van
58359.3483	58359.5221	13.557	0.001	224	DFS
58359.3598	58359.4402	13.591	0.002	138	CDZ
58359.4922	58359.6563	13.536	0.003	81	HaC
58359.6401	58359.7629	13.509	0.001	200	SGE
58359.6418	58359.8195	13.514	0.002	200	SRI
58359.8640	58360.0416	13.519	0.001	526	MGW
58359.9382	58360.1719	1.530	0.004	60	KU2
58359.9389	58360.1696	1.137	0.005	59	KU2
58359.9636	58360.1098	0.698	0.004	40	KU2
58359.9703	58360.0927	0.001	0.006	27	KU2
58360.2615	58360.4011	0.783	0.002	397	MLF

Table E.1: Log of observations of the 2018 outburst in ASASSN-18ey (continued).

Start*	End*	Mag [†]	Error [‡]	N^{\S}	Obs
58360.2819	58360.4577	3.474	0.001	410	Vih
58360.3473	58360.5082	13.631	0.008	85	Van
58360.3819	58360.4909	13.607	0.003	131	CDZ
58360.4929	58360.6560	13.468	0.003	81	HaC
58360.6770	58360.7705	13.521	0.002	140	SGE
58360.9628	58361.1389	13.656	0.004	230	Ioh
58360.9678	58361.0182	1.625	0.003	14	KU2
58360.9685	58361.0189	1.214	0.003	17	KU2
58360.9693	58361.0197	0.788	0.004	16	KU2
58360.9700	58361.0174	0.045	0.006	13	KU2
58361.2736	58361.4197	3.367	0.003	341	Vih
58361.3133	58361.4582	13.501	0.002	340	ATE
58361.3228	58361.4455	13.508	0.003	158	EHE
58361.3477	58361.5123	13.559	0.003	96	Van
58361.3541	58361.4883	13.562	0.002	335	CDZ
58361.4931	58361.6570	13.585	0.003	82	HaC
58361.5573	58361.7489	13.620	0.004	141	UJH
58361.6435	58361.7661	13.597	0.001	200	SGE
58362.2742	58362.4230	0.041	0.006	33	CRI
58362.2750	58362.4422	0.874	0.003	37	CRI
58362.2758	58362.4430	1.262	0.004	37	CRI
58362.2794	58362.4444	1.840	0.009	37	CRI
58362.2876	58362.3258	3.590	0.002	90	Vih
58362.2924	58362.4434	13.626	0.005	98	BSM
58362.3459	58362.5009	13.746	0.007	87	Van
58362.3906	58362.4856	13.666	0.002	238	CDZ
58362.4928	58362.6544	13.482	0.005	81	HaC
58362.5070	58362.6778	13.462	0.003	144	LMA
58362.6555	58362.7780	13.498	0.003	200	SGE
58363.2705	58363.3828	-0.066	0.008	25	CRI
58363.2713	58363.3836	0.714	0.005	25	CRI
58363.2721	58363.3844	1.088	0.005	25	CRI
58363.2757	58363.3859	1.683	0.005	25	CRI
58363.2912	58363.3797	3.430	0.001	207	Vih
58363.3150	58363.4433	13.556	0.003	84	BSM
58363.3509	58363.4785	13.196	0.002	313	CDZ
58363.3663	58363.4959	13.589	0.002	229	Van
58363.5091	58363.6515	13.596	0.003	73	HaC
58363.6669	58363.7309	13.639	0.002	104	SGE
58363.8644	58364.0417	13.490	0.001	527	MGW
58364.0216	58364.1343	1.459	0.007	31	KU2
58364.0223	58364.1350	1.059	0.006	35	KU2
58364.0231	58364.1358	0.653	0.009	29	KU2
58364.0238	58364.1217	-0.046	0.014	20	KU2
58364.2700	58364.4431	13.572	0.004	112	BSM
58364.3225	58364.4466	3.515	0.002	290	Vih
58364.3539	58364.4967	13.764	0.004	81	Van
58364.3564	58364.3993	13.603	0.002	107	CDZ
58364.4932	58364.6488	13.518	0.007	77	HaC
58364.5374	58364.6859	13.477	0.005	123	LMA

Table E.1: Log of observations of the 2018 outburst in ASASSN-18ey (continued).

Start*	End*	Mag [†]	Error [‡]	N [§]	Obs
58364.6343	58364.7671	13.465	0.002	200	SGE
58365.2238	58365.3853	13.923	0.008	53	Zub
58365.2426	58365.3785	0.658	0.003	367	MLF
58365.3487	58365.4769	13.487	0.002	315	CDZ
58365.3563	58365.4683	13.511	0.003	197	Van
58365.4938	58365.6459	13.533	0.003	77	HaC
58365.5498	58365.5841	13.546	0.004	30	LMA
58365.6332	58365.7720	13.545	0.002	125	SGE
58365.8851	58366.0207	13.522	0.003	322	MGW
58366.2917	58366.3907	14.031	0.002	33	Zub
58366.3382	58366.4452	13.609	0.002	132	EHE
58366.3475	58366.4375	13.632	0.002	222	CDZ
58366.3487	58366.4683	13.670	0.002	212	Van
58366.4973	58366.6433	13.616	0.003	61	HaC
58366.5351	58366.6674	13.599	0.003	111	LMA
58366.5556	58366.7356	13.611	0.006	112	UJH
58366.6370	58366.7651	13.549	0.003	200	SGE
58367.0664	58367.1169	1.210	0.007	12	KU2
58367.0687	58367.1369	1.609	0.009	11	KU2
58367.2964	58367.3907	13.602	0.006	63	BSM
58367.3018	58367.3888	14.037	0.005	30	Zub
58367.3312	58367.4295	13.564	0.005	83	EHE
58367.3544	58367.4717	13.541	0.002	288	CDZ
58367.4951	58367.6405	13.512	0.005	60	HaC
58367.6309	58367.7553	13.554	0.001	200	SGE
58368.2860	58368.4136	3.487	0.002	287	Vih
58368.3817	58368.4581	13.712	0.002	124	Van
58368.4968	58368.6375	13.669	0.003	59	HaC
58368.5009	58368.6814	13.669	0.002	135	LMA
58368.6299	58368.7576	13.645	0.004	213	SGE
58368.8653	58369.0405	13.553	0.001	519	MGW
58368.8670	58368.9980	13.593	0.003	149	Nel
58369.2399	58369.4013	3.581	0.001	235	Vih
58369.3163	58369.4193	13.705	0.002	143	EHE
58369.3283	58369.4159	13.983	0.001	174	Van
58369.4983	58369.6349	13.593	0.003	57	HaC
58370.5092	58370.6322	13.726	0.004	47	HaC
58370.5183	58370.6793	13.704	0.002	136	LMA
58370.8847	58371.0351	13.602	0.001	426	MGW
58371.2569	58371.3930	3.568	0.001	317	Vih
58371.2974	58371.3628	0.864	0.002	189	MLF
58371.3803	58371.4577	13.759	0.002	139	Van
58371.4981	58371.6297	13.508	0.005	49	HaC
58372.2536	58372.4223	3.461	0.002	394	Vih
58372.3368	58372.4579	13.661	0.003	208	Van
58372.3392	58372.4529	13.615	0.002	283	CDZ
58372.4975	58372.6271	13.720	0.005	51	HaC
58372.5543	58372.7156	13.786	0.003	124	UJH
58372.6588	58372.7617	13.775	0.002	120	SRI
58372.8650	58373.0210	13.560	0.001	462	MGW

Table E.1: Log of observations of the 2018 outburst in ASASSN-18ey (continued).

Start*	End*	Mag [†]	Error [‡]	N [§]	Obs
58373.2964	58373.4255	13.806	0.004	83	BSM
58373.3427	58373.4573	13.885	0.005	115	Van
58373.4993	58373.6243	13.665	0.008	49	HaC
58373.5495	58373.7137	13.642	0.004	126	UJH
58374.2547	58374.4185	3.424	0.002	383	Vih
58374.2984	58374.3904	13.595	0.003	61	BSM
58374.3372	58374.4522	13.612	0.001	282	CDZ
58374.4994	58374.6194	13.672	0.004	47	HaC
58374.5491	58374.7125	13.738	0.005	127	UJH
58374.8649	58375.0209	13.725	0.002	462	MGW
58375.3046	58375.4405	13.802	0.002	174	EHE
58375.3358	58375.4492	13.844	0.001	284	CDZ
58375.3949	58375.4840	14.006	0.005	130	Van
58375.5014	58375.6192	13.807	0.005	46	HaC
58375.5490	58375.7112	13.810	0.005	117	UJH
58376.3408	58376.4467	13.775	0.004	159	CDZ
58376.5492	58376.7077	13.837	0.004	121	UJH
58376.6697	58376.7504	13.848	0.002	103	SJI
58377.2652	58377.3980	13.728	0.010	78	BSM
58377.3355	58377.4436	13.888	0.002	270	CDZ
58377.5489	58377.7053	13.918	0.004	120	UJH
58377.8656	58378.0158	13.862	0.002	450	MGW
58378.0140	58378.1109	13.866	0.006	132	Ioh
58378.2501	58378.3732	3.727	0.001	288	Vih
58378.3550	58378.4789	13.777	0.003	209	Van
58378.5363	58378.7026	13.823	0.006	122	UJH
58378.5661	58378.6810	13.851	0.004	127	BJA
58378.6216	58378.6746	13.822	0.002	88	SGE
58379.0410	58379.1003	1.822	0.005	17	KU2
58379.0417	58379.1040	1.445	0.007	20	KU2
58379.0425	58379.1047	1.038	0.011	17	KU2
58379.2409	58379.3830	3.684	0.002	332	Vih
58379.3075	58379.4154	13.876	0.002	227	RJW
58379.3090	58379.3779	0.328	0.007	16	CRI
58379.3098	58379.3970	1.138	0.009	20	CRI
58379.3106	58379.3978	1.542	0.009	20	CRI
58379.3121	58379.3856	2.047	0.027	17	CRI
58379.5245	58379.6313	13.953	0.002	123	SDB
58379.5297	58379.6057	13.967	0.007	23	HaC
58379.5388	58379.7005	14.010	0.004	125	UJH
58379.6178	58379.7697	13.985	0.002	250	SGE
58379.8955	58380.0105	13.921	0.001	345	MGW
58380.2619	58380.3972	3.829	0.001	316	Vih
58380.2903	58380.4200	14.010	0.004	156	EHE
58380.5173	58380.6028	13.969	0.006	25	HaC
58380.5727	58380.6394	14.005	0.002	153	SJI
58381.2309	58381.3433	0.373	0.007	25	CRI
58381.2317	58381.3441	1.192	0.006	25	CRI
58381.2325	58381.3449	1.595	0.006	25	CRI
58381.2361	58381.3464	2.178	0.011	25	CRI

Table E.1: Log of observations of the 2018 outburst in ASASSN-18ey (continued).

Start*	End*	Mag [†]	Error [‡]	N [§]	Obs
58381.2471	58381.4000	3.823	0.003	357	Vih
58381.3274	58381.4306	14.105	0.004	213	CDZ
58381.5007	58381.6024	14.077	0.005	33	HaC
58381.5279	58381.6373	14.158	0.004	84	RIT
58381.6186	58381.7067	14.117	0.002	150	SGE
58381.8747	58382.0051	13.968	0.001	276	MGW
58382.2331	58382.3327	1.258	0.005	267	MLF
58382.2376	58382.3426	0.519	0.010	23	CRI
58382.2384	58382.3434	1.318	0.004	21	CRI
58382.2392	58382.3442	1.713	0.005	21	CRI
58382.2498	58382.3457	2.249	0.012	20	CRI
58382.2533	58382.3964	3.967	0.003	318	Vih
58382.4729	58382.6466	13.941	0.006	147	LMA
58382.4959	58382.5972	13.919	0.009	33	HaC
58382.5117	58382.6235	13.889	0.004	240	DKS
58382.5342	58382.6864	13.911	0.006	120	UJH
58382.6231	58382.7567	13.911	0.003	222	SGE
58382.6466	58382.7531	13.911	0.001	243	SJI
58383.2656	58383.3598	0.941	0.009	20	CRI
58383.2709	58383.3606	1.375	0.010	19	CRI
58383.2724	58383.3621	2.026	0.010	19	CRI
58383.2747	58383.3636	0.069	0.009	20	CRI
58383.2773	58383.4161	14.253	0.004	252	Van
58383.2832	58383.3839	14.033	0.007	64	BSM
58383.4994	58383.5945	14.127	0.006	31	HaC
58383.5152	58383.6492	14.131	0.003	253	DKS
58383.6318	58383.7576	14.154	0.004	205	SGE
58383.9022	58384.0913	1.914	0.008	60	KU2
58383.9029	58384.0980	1.539	0.007	59	KU2
58383.9036	58384.0869	1.142	0.007	57	KU2
58383.9073	58384.0758	0.453	0.007	41	KU2
58384.3195	58384.4586	14.136	0.006	128	Van
58384.3239	58384.4248	13.836	0.003	250	CDZ
58384.4760	58384.6348	14.012	0.007	126	LMA
58384.5318	58384.6848	13.974	0.005	116	UJH
58384.5351	58384.6530	13.944	0.004	201	DKS
58384.5524	58384.6635	13.982	0.004	122	BJA
58384.5895	58384.7531	13.950	0.002	376	SJI
58384.6124	58384.7345	13.937	0.002	200	SGE
58384.8745	58384.9309	14.096	0.002	117	MGW
58385.2633	58385.3840	14.009	0.007	78	BSM
58385.2977	58385.3962	13.876	0.002	211	RJW
58385.3230	58385.4215	13.944	0.002	246	CDZ
58385.3304	58385.4511	13.878	0.005	113	Van
58385.4848	58385.6006	13.995	0.008	97	LMA
58385.4996	58385.5889	14.016	0.010	30	HaC
58385.5135	58385.6446	14.109	0.008	41	RIT
58385.5275	58385.6813	14.142	0.007	119	UJH
58385.5538	58385.6602	14.152	0.005	122	BJA
58385.5770	58385.7285	14.166	0.002	348	SJI

Table E.1: Log of observations of the 2018 outburst in ASASSN-18ey (continued).

Start*	End*	Mag [†]	Error [‡]	N^{\S}	Obs
58385.6116	58385.7038	14.162	0.003	150	SGE
58385.8748	58385.9115	14.162	0.004	82	MGW
58386.2392	58386.2654	3.833	0.003	62	Vih
58386.2935	58386.3964	14.135	0.002	220	RJW
58386.3218	58386.4509	14.172	0.004	203	Van
58386.3421	58386.4197	14.226	0.004	81	CDZ
58386.4784	58386.5955	14.077	0.006	75	LMA
58386.5152	58386.5865	14.050	0.007	37	HaC
58386.6105	58386.7033	13.980	0.002	150	SGE
58386.8750	58386.9869	14.060	0.008	98	MGW
58387.3205	58387.4356	14.112	0.005	221	CDZ
58387.3493	58387.4509	14.043	0.007	105	Van
58387.5066	58387.5996	14.048	0.004	46	HaC
58387.5867	58387.6398	14.084	0.004	116	DKS
58387.6145	58387.7367	14.212	0.003	200	SGE
58387.8746	58387.9509	14.271	0.002	156	MGW
58388.2690	58388.3990	14.479	0.006	225	Van
58388.2886	58388.4238	14.196	0.004	287	RJW
58388.3447	58388.4329	14.341	0.008	65	CDZ
58388.5148	58388.5986	14.263	0.011	27	HaC
58388.5510	58388.6589	14.307	0.003	122	BJA
58388.6083	58388.7304	14.255	0.002	200	SGE
58388.8746	58388.9857	14.139	0.001	245	MGW
58388.9719	58389.0733	2.194	0.013	35	KU2
58388.9727	58389.0770	1.826	0.014	36	KU2
58388.9734	58389.0778	1.420	0.012	36	KU2
58388.9741	58389.0637	0.713	0.020	24	KU2
58389.2641	58389.3988	14.658	0.002	242	Van
58389.2875	58389.4125	14.292	0.003	269	RJW
58389.2887	58389.3866	14.305	0.005	65	EHE
58389.3157	58389.4308	14.345	0.003	224	CDZ
58389.3167	58389.4035	14.324	0.004	166	IMi
58389.5153	58389.5956	14.139	0.008	26	HaC
58389.5834	58389.7243	14.269	0.004	178	SJI
58389.6242	58389.7519	14.284	0.006	207	SGE
58389.8971	58389.9813	2.397	0.005	27	KU2
58389.8978	58389.9702	2.003	0.003	25	KU2
58389.8986	58389.9680	1.580	0.005	24	KU2
58389.8993	58389.9687	0.854	0.008	20	KU2
58390.2483	58390.3518	0.467	0.012	22	CRI
58390.2491	58390.3526	1.354	0.007	20	CRI
58390.2499	58390.3534	1.794	0.007	20	CRI
58390.2535	58390.3549	2.416	0.018	23	CRI
58390.2724	58390.3955	14.674	0.003	218	Van
58390.2930	58390.4170	14.350	0.003	265	RJW
58390.3161	58390.4271	14.443	0.004	213	CDZ
58390.4776	58390.5652	14.449	0.004	58	LMA
58390.5198	58390.5916	14.443	0.007	30	HaC
58390.6081	58390.7303	14.508	0.003	200	SGE
58390.6371	58390.6686	14.534	0.015	27	UJH

Table E.1: Log of observations of the 2018 outburst in ASASSN-18ey (continued).

Start*	End*	Mag [†]	Error [‡]	N^{\S}	Obs
58390.9710	58390.9806	14.339	0.007	22	MGW
58391.2277	58391.3037	1.731	0.011	192	MLF
58391.2510	58391.3760	14.640	0.007	57	BSM
58391.2699	58391.3956	14.835	0.002	219	Van
58391.2844	58391.4151	14.504	0.002	284	RJW
58391.3152	58391.4252	14.575	0.002	205	CDZ
58391.4709	58391.6241	14.453	0.005	97	LMA
58391.6371	58391.7194	14.444	0.002	102	SJI
58391.8748	58391.9775	14.541	0.003	229	MGW
58392.2332	58392.3314	2.517	0.020	22	CRI
58392.2340	58392.3276	2.514	0.025	20	CRI
58392.2348	58392.3284	2.511	0.018	20	CRI
58392.2384	58392.3299	2.460	0.014	20	CRI
58392.2600	58392.3763	14.521	0.005	53	BSM
58392.3151	58392.4221	14.492	0.003	194	CDZ
58392.5095	58392.5860	14.584	0.008	31	HaC
58392.5149	58392.6250	14.585	0.003	228	DKS
58392.8747	58392.9750	14.481	0.004	126	MGW
58392.9269	58393.0779	2.438	0.011	41	KU2
58392.9276	58393.0787	2.067	0.010	48	KU2
58392.9283	58393.0645	1.651	0.014	39	KU2
58392.9291	58393.0416	0.926	0.011	17	KU2
58393.3212	58393.4304	14.709	0.004	140	Van
58393.3293	58393.3913	14.813	0.004	96	CDZ
58393.4642	58393.6031	14.658	0.003	91	LMA
58393.5131	58393.5831	14.665	0.007	27	HaC
58393.8750	58393.9701	14.690	0.002	120	MGW
58394.3117	58394.4166	14.553	0.004	204	CDZ
58394.3569	58394.4312	14.499	0.006	91	Van
58394.5177	58394.5802	14.673	0.008	23	HaC
58395.3106	58395.4139	14.839	0.003	201	CDZ
58395.3377	58395.4315	14.769	0.004	126	Van
58395.5104	58395.5778	14.698	0.009	26	HaC
58395.5249	58395.5766	14.687	0.012	30	UJH
58395.5322	58395.6139	14.665	0.003	140	DKS
58396.3095	58396.4112	14.697	0.004	198	CDZ
58396.3371	58396.4313	14.631	0.007	115	Van
58396.5152	58396.5761	14.564	0.006	18	HaC
58396.5280	58396.6456	14.650	0.009	80	UJH
58396.6110	58396.7051	14.733	0.004	120	SJI
58397.2267	58397.2974	4.410	0.003	92	Vih
58397.2448	58397.3370	2.106	0.015	17	CRI
58397.2503	58397.3348	0.755	0.016	16	CRI
58397.2514	58397.3359	1.676	0.014	16	CRI
58397.2542	58397.3387	2.672	0.024	16	CRI
58397.2586	58397.3620	14.748	0.006	47	BSM
58397.3079	58397.4086	14.762	0.004	196	CDZ
58397.3397	58397.4398	14.642	0.005	78	EHE
58397.3423	58397.4311	14.942	0.003	121	Van
58397.5152	58397.5735	14.744	0.027	13	HaC

Table E.1: Log of observations of the 2018 outburst in ASASSN-18ey (continued).

Start*	End*	Mag [†]	Error [‡]	N^{\S}	Obs
58397.5876	58397.7044	14.645	0.006	141	SJI
58397.8928	58397.9730	14.509	0.006	49	Nel
58397.9129	58398.0153	14.446	0.010	78	Ioh
58397.9162	58397.9587	14.440	0.005	54	MGW
58398.2232	58398.3349	0.716	0.009	19	CRI
58398.2244	58398.3360	1.552	0.009	19	CRI
58398.2255	58398.3372	1.985	0.012	19	CRI
58398.2294	58398.3388	2.459	0.025	19	CRI
58398.3364	58398.4032	14.666	0.004	84	Van
58398.5990	58398.7075	14.380	0.004	173	SGE
58399.2208	58399.3299	0.387	0.010	20	CRI
58399.2220	58399.3310	1.212	0.007	20	CRI
58399.2231	58399.3322	1.598	0.008	20	CRI
58399.2269	58399.3339	2.021	0.008	20	CRI
58399.2552	58399.3391	14.260	0.006	32	BSM
58399.3228	58399.4162	14.368	0.006	101	Van
58399.6206	58399.7159	14.309	0.007	102	SGE
58399.9002	58400.0389	1.960	0.006	44	KU2
58399.9009	58400.0515	1.715	0.006	48	KU2
58399.9016	58400.0404	1.385	0.006	44	KU2
58399.9053	58399.9877	0.750	0.011	26	KU2
58400.2371	58400.3439	4.098	0.003	135	Vih
58400.2582	58400.3269	1.846	0.014	15	CRI
58400.2598	58400.3284	2.296	0.022	15	CRI
58400.2657	58400.3299	0.670	0.022	15	CRI
58400.2665	58400.3261	1.479	0.009	14	CRI
58400.4744	58400.5659	14.253	0.007	44	HaC
58400.5195	58400.6366	14.229	0.008	91	UJH
58400.6133	58400.7119	14.130	0.002	153	SGE
58400.8751	58400.9448	14.256	0.004	84	MGW
58400.8915	58401.0250	1.962	0.008	40	KU2
58400.8923	58401.0287	1.730	0.006	42	KU2
58400.8960	58401.0265	1.410	0.008	39	KU2
58400.9032	58400.9867	14.421	0.008	156	Kis
58400.9056	58400.9797	0.837	0.008	20	KU2
58401.2366	58401.3334	14.153	0.005	44	BSM
58401.2738	58401.3637	14.295	0.003	138	Van
58401.6199	58401.7050	14.179	0.003	101	SGE
58402.2588	58402.3510	14.178	0.005	65	EHE
58402.2767	58402.3132	14.196	0.005	49	IMi
58402.3026	58402.3643	14.356	0.008	135	Van
58402.4741	58402.5438	14.149	0.006	47	HaC
58402.5977	58402.6834	14.112	0.002	100	SGE
58402.6103	58402.7044	14.110	0.003	93	SJI
58403.1786	58403.3237	0.482	0.027	25	CRI
58403.1794	58403.3153	1.220	0.018	30	CRI
58403.1802	58403.3161	1.577	0.014	30	CRI
58403.1824	58403.3176	2.049	0.029	26	CRI
58403.2170	58403.3337	3.910	0.002	151	Vih
58403.2593	58403.3158	14.138	0.004	46	EHE

Table E.1: Log of observations of the 2018 outburst in ASASSN-18ey (continued).

Start*	End*	Mag [†]	Error [‡]	N^{\S}	Obs
58403.4747	58403.5418	14.188	0.004	46	HaC
58403.5630	58403.6256	14.254	0.007	42	UJH
58403.6399	58403.7222	14.250	0.003	95	SGE
58404.2374	58404.3359	0.428	0.017	22	CRI
58404.2374	58404.3359	0.428	0.017	22	Vih
58404.2382	58404.3367	1.155	0.008	22	CRI
58404.2390	58404.3329	1.509	0.008	18	CRI
58404.2426	58404.3344	1.937	0.018	20	CRI
58404.4748	58404.5390	14.152	0.005	44	HaC
58404.5958	58404.6904	14.042	0.003	108	SGE
58404.6173	58404.6294	14.077	0.011	11	UJH
58405.1969	58405.3297	3.844	0.002	172	Vih
58405.4771	58405.5354	14.134	0.004	36	HaC
58405.6123	58405.7010	14.147	0.004	100	SGE
58405.9283	58405.9787	1.659	0.009	13	KU2
58405.9290	58405.9794	1.326	0.015	13	KU2
58405.9305	58405.9809	1.902	0.009	13	KU2
58406.4783	58406.5331	14.205	0.005	25	HaC
58406.6020	58406.6837	14.166	0.003	100	SGE
58406.8799	58406.9629	0.699	0.018	14	KU2
58406.8806	58406.9726	1.913	0.006	30	KU2
58406.8814	58406.9733	1.680	0.008	27	KU2
58406.8821	58406.9681	1.341	0.008	25	KU2
58407.2014	58407.3288	3.971	0.002	165	Vih
58407.2998	58407.3445	14.200	0.006	34	EHE
58407.4786	58407.5302	14.191	0.005	24	HaC
58408.1606	58408.3242	0.794	0.009	31	CRI
58408.1606	58408.3242	0.794	0.009	31	Vih
58408.1614	58408.3113	1.501	0.009	32	CRI
58408.1622	58408.3213	1.818	0.010	34	CRI
58408.1644	58408.2998	2.175	0.016	30	CRI
58408.2001	58408.3260	3.915	0.002	163	Vih
58408.2977	58408.3874	14.214	0.005	109	Van
58408.4786	58408.5265	14.238	0.006	17	HaC
58408.5923	58408.6978	14.230	0.004	100	SGE
58408.8787	58408.9495	0.753	0.010	20	KU2
58408.8802	58409.0423	1.718	0.006	31	KU2
58408.8809	58409.0342	1.380	0.008	27	KU2
58408.8825	58409.0446	1.968	0.007	29	KU2
58409.1728	58409.2997	0.850	0.011	27	CRI
58409.1728	58409.2997	0.850	0.011	27	Vih
58409.1736	58409.3051	1.563	0.011	28	CRI
58409.1744	58409.3013	1.860	0.009	28	CRI
58409.1766	58409.2982	2.229	0.015	25	CRI
58409.1963	58409.3182	3.968	0.002	158	Vih
58409.4791	58409.5244	14.223	0.006	21	HaC
58409.5992	58409.6532	14.184	0.003	50	SGE
58410.2824	58410.3398	14.459	0.003	87	Van
58410.4798	58410.5210	14.225	0.007	19	HaC
58410.6335	58410.6900	14.275	0.004	50	SGE

Table E.1: Log of observations of the 2018 outburst in ASASSN-18ey (continued).

Start*	End*	Mag [†]	Error [‡]	N^{\S}	Obs
58410.8711	58410.9710	0.823	0.014	29	KU2
58410.8734	58411.0177	1.473	0.006	46	KU2
58410.8779	58411.0192	2.041	0.005	48	KU2
58410.8786	58411.0319	1.793	0.005	49	KU2
58411.4799	58411.5186	14.257	0.009	18	HaC
58411.5902	58411.6700	14.258	0.005	50	SGE
58411.9043	58412.0146	2.069	0.006	36	KU2
58411.9050	58412.0183	1.824	0.007	38	KU2
58411.9057	58412.0131	1.487	0.006	36	KU2
58411.9094	58411.9842	0.868	0.010	23	KU2
58412.2316	58412.3326	14.581	0.003	135	Van
58412.4793	58412.5157	14.293	0.014	26	HaC
58412.5895	58412.6882	14.334	0.004	53	SGE
58412.8696	58413.0092	1.497	0.006	44	KU2
58412.8711	58412.9537	14.273	0.015	105	Kis
58412.8711	58413.0047	2.102	0.008	45	KU2
58412.8719	58413.0084	1.841	0.007	45	KU2
58412.8733	58412.9743	0.879	0.009	33	KU2
58412.8950	58413.0099	14.454	0.010	173	Ioh
58413.2387	58413.3328	14.587	0.003	130	Van
58413.4795	58413.5147	14.394	0.005	60	HaC
58413.6140	58413.6892	14.348	0.004	50	SGE
58413.8958	58413.9581	1.611	0.026	17	KU2
58413.8980	58413.9574	1.962	0.026	18	KU2
58413.9003	58413.9626	2.204	0.022	18	KU2
58414.2933	58414.3643	14.452	0.009	84	Van
58414.4798	58414.5120	14.441	0.006	55	HaC
58414.6005	58414.6781	14.440	0.004	50	SGE
58415.4803	58415.5090	14.487	0.010	49	HaC
58415.9824	58416.0149	0.058	0.010	38	KU3
58416.2451	58416.3110	14.558	0.014	29	BSM
58416.3317	58416.3727	14.664	0.007	55	Van
58416.4805	58416.5061	14.538	0.008	44	HaC
58416.5857	58416.6722	14.467	0.005	65	SGE
58416.9865	58417.0183	0.030	0.011	45	KU3
58417.4805	58417.5038	14.580	0.010	40	HaC
58418.4811	58418.5008	14.602	0.010	34	HaC
58418.6067	58418.6817	14.606	0.005	50	SGE
58419.3490	58419.3710	14.892	0.010	30	Van
58419.4813	58419.4980	14.674	0.012	29	HaC
58419.8755	58419.9970	0.223	0.004	155	KU3
58419.8937	58419.9909	14.808	0.010	152	Ioh
58420.1666	58420.2899	1.905	0.012	26	CRI
58420.1666	58420.2899	1.905	0.012	26	Vih
58420.1681	58420.2907	2.236	0.012	26	CRI
58420.1681	58420.2907	2.236	0.012	26	Vih
58420.1718	58420.2922	2.546	0.018	22	CRI
58420.1718	58420.2922	2.546	0.018	22	Vih
58420.2906	58420.3571	14.787	0.010	85	Van
58420.4823	58420.4955	14.580	0.012	23	HaC

Table E.1: Log of observations of the 2018 outburst in ASASSN-18ey (continued).

Start*	End*	Mag [†]	Error [‡]	N [§]	Obs
58420.8670	58420.9873	0.221	0.004	163	KU3
58421.4828	58421.4923	14.714	0.016	17	HaC
58421.6064	58421.6214	14.677	0.011	15	SGE
58421.8985	58422.0082	0.238	0.005	148	KU3
58422.3238	58422.3568	14.936	0.008	37	Van
58422.4830	58422.4895	14.719	0.026	12	HaC
58422.8811	58422.9101	0.296	0.010	24	KU3
58423.1780	58423.2766	4.425	0.004	68	Vih
58424.2942	58424.3460	15.057	0.007	69	Van
58425.2450	58425.2763	15.109	0.007	46	Van
58425.2922	58425.3465	15.117	0.009	65	Van
58425.8638	58425.9968	0.411	0.006	163	KU3
58425.8825	58425.9948	15.015	0.014	136	Ioh
58426.2920	58426.3468	15.136	0.005	80	Van
58427.2310	58427.2914	15.158	0.005	93	Van
58428.8790	58428.9653	0.560	0.006	105	KU3
58430.1774	58430.2466	4.865	0.006	90	Vih
58431.5815	58431.6480	15.198	0.011	61	SGE
58432.1815	58432.2444	5.068	0.007	81	Vih
58432.5813	58432.6177	15.217	0.012	30	SGE
58436.4808	58436.5477	15.644	0.041	53	UJH
58437.4804	58437.5454	15.595	0.019	54	UJH
58439.1719	58439.2028	5.208	0.012	22	Vih
58440.2226	58440.3025	16.067	0.009	121	Van
58441.2226	58441.2932	16.088	0.008	107	Van

*BJD – 2400000.0.

†Mean magnitude.

‡ 1σ of mean magnitude.

§Number of observations.

||Observer's code: ATE[#] (T.Arranz), BJA[#] (B.James), BMS[#] (M.Bundas), BSM (S.M.Brincat), CDJ[#] (D.Coulter), CDZ[#] (D.C.Fernandez), COO (L.M.Cook), CRI (Crimean Astrophys.Obs), deM (E.de Miguel), DFS[#] (S.Dufoer), DJE[#] (J.-B.Desrosiers), DKS (S.Dvorak), EEY[#] (E.Erdelyi), EHE[#] (H.-B.Eggenstein), GCH (C.Galdies), HaC (F.-J.Hamsch), HBB[#] (B.Harris), IMi (I.Miller), Ioh (H.Itoh), JJI[#] (J.Jones), Kis (S.Kiyota), KU1 (Kyoto Univ. Team), KU2 (Kyoto Univ. Team), KU3 (Kyoto Univ. Team), LCO (C.Littlefield), Lic (D.Licchelli), Lis (Lisniki Obs.team), LMA[#] (D.Lemay), LPA[#] (P.Lewin), MGW (G.Myers), MLF (B.Monard), MZK (K.Menzies), Nel (P.Nelson), NOM[#] (O.Noroozi), OAR (A.Oksanen), OYE (Y.Ögmen), PXR (R.D.Pickard), RIT (M.Richmond), RJW[#] (J.Rock), SDB (D.Starkey), SGE (G.Stone), SJI[#] (J.Seargeant), SJP[#] (J.Seitz), SRI (R.Sabo), Trt (T.Tordai), UJH (J.Ulowetz), Van (T.Vanmunster), Vih (Vihorlat Obs.team), and Zub (A.M.Zubareva)

#Inclusive of observations from the AAVSO database.

Table E.2: Times of superhump maxima in ASASSN-18ey.

E^*	Max [†]	Error	$O - C^{\ddagger}$	N^{\S}
0	58279.8440	0.0033	-0.0870	731
1	58280.4646	0.0009	-0.1553	683
2	58281.1999	0.0074	-0.1089	489
3	58281.8491	0.0016	-0.1486	917
4	58282.5680	0.0010	-0.1186	623
5	58283.3621	0.0009	-0.0134	1123
7	58284.6721	0.0009	-0.0812	1882
8	58285.3527	0.0018	-0.0895	936
10	58286.7878	0.0009	-0.0322	878
11	58287.4605	0.0011	-0.0484	1306
13	58288.8796	0.0012	-0.0072	393
14	58289.5798	0.0006	0.0041	1665
16	58290.9428	0.0010	-0.0107	1530
17	58291.6576	0.0003	0.0152	4396
18	58292.3645	0.0006	0.0331	2454
19	58292.9832	0.0019	-0.0370	1398
20	58293.7083	0.0005	-0.0009	2812
21	58294.4226	0.0009	0.0245	691
22	58295.1171	0.0008	0.0301	1214
23	58295.8055	0.0004	0.0297	3264
24	58296.4778	0.0005	0.0130	584
25	58297.1990	0.0012	0.0454	864
26	58297.8601	0.0016	0.0176	1004
27	58298.5326	0.0004	0.0011	2142
28	58299.2309	0.0019	0.0105	1241
29	58299.9187	0.0008	0.0094	820
30	58300.6085	0.0006	0.0103	1372
31	58301.3099	0.0006	0.0228	1615
32	58301.9511	0.0039	-0.0249	453
33	58302.6849	0.0006	0.0199	4059
34	58303.3695	0.0004	0.0157	3498
35	58304.0612	0.0012	0.0185	1097
36	58304.7386	0.0009	0.0070	1275
37	58305.4216	0.0005	0.0011	1105
38	58306.1185	0.0008	0.0090	345
39	58306.8089	0.0008	0.0106	2065
40	58307.5062	0.0003	0.0189	5938
41	58308.1783	0.0049	0.0021	1337
42	58308.8848	0.0011	0.0197	1535
43	58309.5536	0.0005	-0.0004	3288
44	58310.2385	0.0009	-0.0044	3582
45	58310.9671	0.0018	0.0353	1461
46	58311.6123	0.0006	-0.0084	3549
47	58312.3225	0.0006	0.0129	3212
48	58313.0023	0.0004	0.0037	2844
49	58313.6892	0.0021	0.0018	3482
50	58314.3994	0.0002	0.0231	3916
51	58315.0608	0.0005	-0.0045	3376
52	58315.7464	0.0005	-0.0077	2118
53	58316.4302	0.0006	-0.0129	3761
54	58317.0843	0.0030	-0.0477	2379
55	58317.7866	0.0007	-0.0343	2336
56	58318.5029	0.0004	-0.0069	3919

Table E.1: Times of superhump maxima in ASASSN-18ey (continued).

E^*	Max [†]	Error	$O - C^{\ddagger}$	N^{\S}
57	58319.2593	0.0009	0.0606	3039
58	58319.8660	0.0005	-0.0216	2394
59	58320.5493	0.0012	-0.0272	1144
60	58321.2636	0.0008	-0.0018	1927
61	58321.9246	0.0006	-0.0298	2198
62	58322.6273	0.0005	-0.0159	2725
63	58323.3158	0.0019	-0.0164	2081
64	58323.9921	0.0010	-0.0290	2544
65	58324.6795	0.0005	-0.0305	1861
66	58325.3605	0.0006	-0.0384	1551
67	58326.1272	0.0009	0.0394	848
68	58326.7252	0.0013	-0.0515	1175
69	58327.4221	0.0008	-0.0435	1295
70	58328.3213	0.0028	0.1668	625
71	58328.8184	0.0015	-0.0250	680
74	58330.9403	0.0019	0.0302	1539
75	58331.5725	0.0044	-0.0266	1485
76	58332.2482	0.0009	-0.0398	2118
77	58332.9434	0.0030	-0.0335	1463
79	58334.3370	0.0014	-0.0177	2392
82	58336.3719	0.0010	-0.0494	2219
84	58337.7828	0.0018	-0.0164	1271
85	58338.4287	0.0006	-0.0594	1575
87	58339.8917	0.0017	0.0258	1255
88	58340.5428	0.0022	-0.0121	1367
89	58341.2138	0.0156	-0.0299	624
90	58341.9208	0.0025	-0.0119	442
91	58342.5845	0.0019	-0.0370	1019
92	58343.3115	0.0018	0.0011	752
93	58343.9752	0.0014	-0.0241	881
94	58344.6792	0.0095	-0.0090	934
95	58345.3455	0.0013	-0.0317	1044
96	58345.9794	0.0036	-0.0867	250
97	58346.7364	0.0013	-0.0186	754
98	58347.3908	0.0011	-0.0531	999
99	58348.2862	0.0031	0.1534	1761
100	58348.7940	0.0129	-0.0277	163
101	58349.4683	0.0019	-0.0423	1079
102	58350.2421	0.0016	0.0425	851
103	58350.8677	0.0014	-0.0207	620
104	58351.5276	0.0101	-0.0498	1112
105	58352.2088	0.0020	-0.0574	838
106	58352.9177	0.0013	-0.0374	1153
108	58354.2435	0.0029	-0.0894	1003
109	58354.9403	0.0031	-0.0816	438
110	58355.6706	0.0026	-0.0402	394
111	58356.3365	0.0023	-0.0632	731
112	58357.0832	0.0056	-0.0054	606
113	58357.8102	0.0041	0.0327	996
114	58358.3519	0.0026	-0.1145	1271
115	58359.1580	0.0052	0.0026	899
116	58359.7641	0.0016	-0.0801	1130
117	58360.5560	0.0041	0.0228	1190

Table E.1: Times of superhump maxima in ASASSN-18ey (continued).

E^*	Max [†]	Error	$O - C^{\ddagger}$	N^{\S}
118	58361.2027	0.0032	-0.0193	1511
120	58362.5710	0.0016	-0.0288	1043
121	58363.2287	0.0072	-0.0600	932
122	58363.9226	0.0019	-0.0550	750
123	58364.6181	0.0026	-0.0485	946
124	58365.3381	0.0017	-0.0174	1022
125	58366.0460	0.0028	0.0016	335
126	58366.7054	0.0049	-0.0279	483
127	58367.4575	0.0013	0.0353	658
128	58368.1344	0.0070	0.0233	203
129	58368.8274	0.0026	0.0274	1024
130	58369.5051	0.0043	0.0162	360
132	58370.8360	0.0023	-0.0307	557
133	58371.5017	0.0022	-0.0539	694
134	58372.3004	0.0020	0.0558	933
135	58372.8950	0.0013	-0.0384	657
136	58373.5796	0.0026	-0.0428	225
137	58374.2969	0.0012	-0.0143	774
138	58375.0374	0.0040	0.0372	462
139	58375.6161	0.0074	-0.0730	250
140	58376.3044	0.0027	-0.0736	159
141	58377.1200	0.0078	0.0531	348
142	58377.7305	0.0024	-0.0254	542
143	58378.4207	0.0012	-0.0241	827
144	58379.1409	0.0021	0.0073	693
145	58379.8095	0.0032	-0.0130	591
146	58380.5242	0.0269	0.0127	650
147	58381.2222	0.0028	0.0219	670
148	58381.9014	0.0028	0.0121	428
149	58382.5722	0.0012	-0.0060	1357
153	58385.3574	0.0017	0.0236	1146
154	58386.0454	0.0114	0.0227	211
155	58386.6769	0.0052	-0.0347	513
156	58387.4058	0.0020	0.0053	589
157	58388.0643	0.0065	-0.0251	298
158	58388.7925	0.0038	0.0142	716
159	58389.4861	0.0015	0.0188	1377
160	58390.1198	0.0174	-0.0363	766
161	58390.8275	0.0084	-0.0176	123
162	58391.5608	0.0042	0.0269	936
163	58392.2439	0.0061	0.0210	367
164	58392.8591	0.0103	-0.0527	316
166	58394.3084	0.0055	0.0189	327
169	58396.4118	0.0014	0.0555	505
173	58399.1115	0.0205	-0.0004	213
174	58399.9509	0.0149	0.1501	240
175	58400.6384	0.0048	0.1486	351
176	58401.1023	0.0058	-0.0764	583
181	58404.7732	0.0035	0.1500	190

*Cycle counts.

†BJD-2400000.0.

‡ $C = 2458261.952323 + 0.688907 E$.

§Number of points used for determining the maximum.